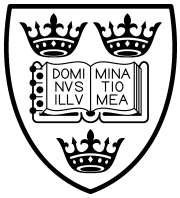
The effects of ionic surfactants on expanding free surfaces



Alexander J.P. White

Wadham College

University of Oxford

A thesis submitted for the degree of

MSc in Mathematical Modelling and Scientific Computing

Trinity 2001

Acknowledgements

I would like to thank my supervisor Dr Chris Breward for helping me over the past few months and for making valuable contributions of time and support. I would also like to deeply thank Dr Kathryn Harriman for her patience in helping me with my numerical work and LaTeX . Their tolerance, advice and encouragement have been fundamental to me completing this work. I would also like to acknowledge Dr Peter Howell for kindly donating the numerical scheme used in Section 4.1.1 of this work; and to the EPSRC for providing me with funding for this year.

I would also like to thank all my friends at Wadham and those I have made this year during the MSc for providing me with a little light relief away from my studies at every opportunity.

Finally, a huge thank you goes to my girlfriend and to my family for their encouragement and support and for always supplying me with a bit of extra cash whenever I was short.

Abstract

This study is based upon the "overflowing cylinder" experiment and develops an ionic theory for the advection-diffusion dynamics of surfactant in this experiment. It is hoped that a consideration of these ionic effects can account for discrepancies between theoretical and experimental results for the overflowing cylinder.

We begin by describing in detail the general fluid and surfactant dynamics and produce a model for this ionic system. We apply the model to a range of different problems to gain an understanding of the ionic effects.

Finally, we address the original nonionic model presented for the analysis of the overflowing cylinder experiment and decipher a parameter missing from some papers which study this experiment.

Contents

1 Introduction **6**

2 Physical Background **10**

2.1 Fluid Dynamics 10

2.2 Surfactant Dynamics 11

2.3 Physical Data 13

3 The static, steady-state problem **15**

4 The static, time-dependent problem **23**

4.1 The nonionic case 23

4.1.1 Numerical scheme for the Abel equations 27

4.1.2 Numerical scheme for the diffusion equation 29

4.1.3 Discussion of results 33

4.2 The ionic case 35

4.2.1 Matched asymptotics 36

4.2.2 The Abel equations and the numerical scheme 39

4.2.3 Discussion of results 40

5 The non-static, steady-state nonionic problem **44**

5.1 Numerical scheme 48

5.1.1 Discussion of results 49

6 Conclusions & Discussion **55**

A Numerical scheme for the nonionic Abel equations **57**

B Numerical scheme for the diffusion equation **60**

C Numerical scheme for the ionic Abel equations **62**

D Numerical scheme for the non-static, steady-state nonionic problem **66**

Chapter 1

Introduction

This project studies the effect that an ionic surface active agent (or *surfactant*) has on an expanding free surface. Its origins stem from attempts to develop a systematic model for the flow observed in the so-called "overflowing cylinder" experiment. In this experiment, carried out under steady-state conditions and consisting of an open vertical cylinder brimful of water which gently overflows due to a deeply submerged pump, it can be shown that the addition of a small volume concentration of a soluble surfactant increases the overflow velocity of the free surface flow in a dramatic way (sometimes by a factor as large as 10) (see Manning-Benson, Bain, and Darton [13], Manning-Benson, Parker, Bain, and Penfold [15], Manning-Benson, Bain, Darton, Sharpe, Eastoe, and Reynolds [14]). This surprising observation is the subject of discussion in Breward, Darton, Howell, and Ockendon [7] where they note that the increase in overflow velocity is largely attributed to the surfactant generating shear forces at the free surface which accelerate the fluid flow. Developing a systematic theory for the flow using a non-ionic model for the surfactant, Breward, *et al.* [7] calculated values for the dilatation rate for differing values of the bulk concentration and compared these with actual experimental data (see Figure 1.1). While it is clear that theoretical and experimental data do not agree, it is of some consolation that many of the model predictions are of the same order of magnitude as their experimental counterparts; giving a reasonable correlation between the two sets of values for larger bulk concentrations and then a sudden divergence of values at very low concentrations. This gives us food for thought: the fundamental model produced by Breward *et al.* [7], whilst obviously correct in its interpretation of the fluid dynamics in the system, is overlooking some crucial analysis in its model of the surfactant. It is, therefore, hoped that the introduction of ionic effects into the model for the surfactant will remove any discrepancies between theoretical and experimental results.

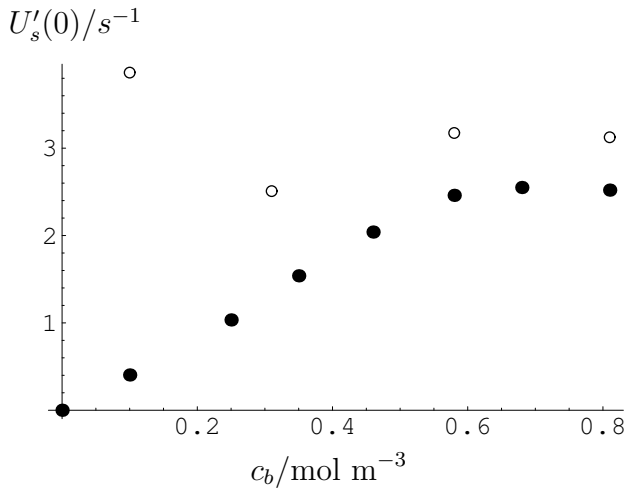


Figure 1.1: Dilatation rate $U_s'(0)$ versus bulk concentration c_b. The closed circles are experimental data whilst the open circles are theoretical predictions.

To develop an ionic model of surfactant dynamics, it is essential to establish a firm understanding of the underlying diffusion and adsorption processes occurring in an aqueous solution. For the most part then, our aim is to obtain a model and investigate the behaviour of an ionic surfactant at an air-water interface. The absorption of ionic surfactants at air-water interfaces has been investigated theoretically in numerous papers (see Vlahovska, Krassimir, Mehreteab and Broze [22]; Chang and Franses [8]; Vakarelski and Dushkin [21]; Geeraerts, Joos and Villé [11];Datwani and Stebe [9]; Mulqueen and Blankschtein [16])). We consider an aqueous solution of cationic (containing positively charged ions) surfactant and its counterions (anions) but with no extra added salt, so that the solution is overall neutrally charged. All ions are treated as point charges.

On addition of a soluble ionic surfactant to a solvent such as water, the dissolved ions are attracted preferentially to the surface where, in the absence of any fluid motion, the cations (attached to a hydrophobic hydrocarbon chain) are adsorbed and reside in a monolayer with a uniform surface concentration, creating a single, two-dimensional charge layer (see Figure 1.2). The evolution of the surface tension at the fluid interface depends upon the rate that these charged species adsorb onto the interface. The adsorption of cations onto the surface is an energetically favourable process for the system provided that the surfactant is below its *critical micelle concentration* (CMC). These micelles are colloidal aggregates of the positively charged cations bound together by the interaction of their hydrophobic chains. The CMC is then the characteristic concentration of surfactant above which the appearance and

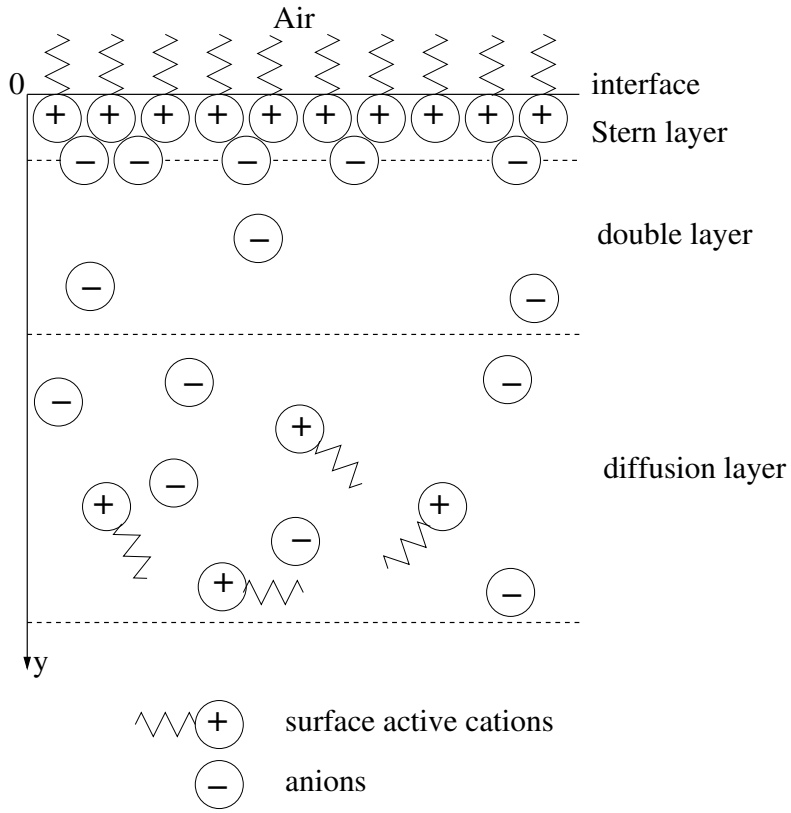


Figure 1.2: Model of the diffusion and the adsorption of cationic surfactant species on a charged interface.

development of these micelles brings about sudden varaiations in the relation between the concentration and certain physico-chemical properties of the solution (such as the surface tension). We therefore consider a surfactant below its CMC so that there is no CMC-generated kinetic barrier to adsorption at the surface.

It takes a finite time for the adsorption of surface cations to reach its equilibrium, given subsurface concentrations of cations and anions $c_{\pm s}$. Note that we assume from the start that no anions adsorb at the surface. The dynamic adsorption behaviour is governed by a two-step process: (1) the transfer of cations between the surface layer and the subsurface layer (the layer immediately below the surface layer, at a thickness of a few ionic diameters only); (2) the exchange of ions between the subsurface and the bulk solution in which they have concentrations $c_{\pm}$. The first step is an adsorption process and the second step is a bulk mass transfer process, i.e. diffusion. The subsurface is the boundary between the domain in which only diffusion occurs and the region in which only adsorption occurs. When cations are adsorbed from the solution to the new interface ($\Gamma = 0$), the concentration first decreases in the subsurface. Diffusion then tends to restore the initial concentration in the subsurface

by bringing ions from the bulk solution. The domain in which diffusion takes place is much larger than the thickness of the adsorption layer.

The constant accumulation of repulsive surface charge density creates an electric potential which, in turn, leads to the formation of an electrical double layer within the solution and slows the rate of subsequent adsorption. The electrostatic description of the system may be further refined by including a *Stern layer* (see Adamson [3], and Schriver, Atkins and Langford [20]); that is, a region in which the counterions bond at the interface and "neutralise" the cations thus reducing the total surface charge.

Another interesting point that arose from Breward *et al.* [7] is that they were unable to fix one parameter in their solution, namely the surfactant concentration at the centre of the overflowing cylinder. They conjectured that the diffusive nature of the surfactant was responsible for transmitting information from the rim of the cylinder and thus it was rim effects (which were neglected in Breward *et al.* [7]) which were responsible for determining the centre concentration. Our second aim, therefore, is to generate numerical simulations of the governing equations (for a nonionc surfactant) on a finite domain to see if, by fixing a plausible boundary condition at the edge (for example, the surface concentration is zero) the centre concentration is uniquely determined.

The remainder of this paper is organised as follows. In Chapter 2, we present the fluid dynamics of our system, and the theory of diffusion of the two types of ions in solution and the electrical potential which influences their behaviour. In Chapter 3, we address the steady-state, static problem. Chapter 4 then uses the results obtained in Chapter 3 to look at the static time-dependent problem. In Chapter 5, we address the nonionic nonstatic problem and decipher the parameter which was missing from the analysis presented in Breward *et al.* [7]. In Chapter 6, we present concluding remarks. The numerical schemes used in this study may be found in the Appendix section at the end.

Chapter 2

Physical Background

2.1 Fluid Dynamics

The ultimate aim of this study is to produce a model for the overflowing cylinder which theoretically predicts the surface velocity and concentrations of ions in solution, just from a knowlegde of the pump velocity U_p, the cylinder radius a and the physical and chemical properties of the surfactant solution, such as its density ρ and dynamic viscosity μ, both of which are assumed to be constant. The fluid dynamics required to model the aqueous solution are well established and are governed by the Navier-Stokes equations

$$\rho\left(\frac{\partial \mathbf{u}}{\partial t} + \mathbf{u}\cdot\nabla\mathbf{u}\right) = -\nabla p + \mu\nabla^2\mathbf{u}, \tag{2.1}$$

$$\nabla\cdot\mathbf{u} = 0, \tag{2.2}$$

with water velocity $\mathbf{u}$ and pressure p.

The over-flowing cylinder experiment has an axisymmetric flow due to the symmetry in the apparatus. It is therefore appropriate to adopt cylindrical polar coordinates (x, y), with x measuring the radial distance away from the axis of the cylinder and the y-axis pointing vertically upwards from the free-surface of the cylinder. The velocity can then be split into two components: u in the x-direction and v in the y-direction.

We assume symmetry at the centre line of the cylinder, so that the radial component of velocity is zero, and at depth in the cylinder, the flow approximates a vertical plug flow. We assume that the free surface is flat so that the kinematic condition tells us that the vertical component of velocity is zero at the free surface. The boundary conditions for the fluid flow are then

$$u = 0 \quad \text{on } x = 0, \quad y < 0, \tag{2.3}$$

$$v = 0 \quad \text{on } y = 0, \tag{2.4}$$

$$u \to 0, \quad v \to U_p \quad \text{as } y \to -\infty. \tag{2.5}$$

Since the free surface is located at $y = 0$, all normal stress conditions on the free surface may be ignored and then neither gravity nor capillarity can play any part in our modelling. Only the tangential free surface stress condition remains which represents a balance between viscous traction and the *Marangoni stress* due to a gradient in the surface tension γ

$$\mu \frac{\partial u}{\partial y} = \frac{d\gamma}{dx} \quad \text{on } y = 0. \tag{2.6}$$

As we shall later see, condition (2.6) provides a coupling between the fluid motion and the surfactant dynamics.

2.2 Surfactant Dynamics

In our model, we consider an aqueous solution of symmetrical ionic surfactant in the absence of any additional salt. We allow for fluid motion and although this experiment is carried out under steady-state conditions it is best to develop first a time-dependent model to give a full understanding of the surfactant dynamics. The transport of the surface active cations with valence q and diffusion coefficient D_+ under the influence of an electrical potential ϕ is described by

$$\frac{\partial c_+}{\partial t} + \mathbf{u} \cdot \nabla c_+ = D_+ \nabla^2 c_+ + \frac{Fq}{RT} D_+ \nabla \cdot (c_+ \nabla \phi). \tag{2.7}$$

Likewise, the transport of the counterions (anions) with valence $-q$ and diffusion coefficient D_- under the influence of the electrical potential ϕ is described by

$$\frac{\partial c_-}{\partial t} + \mathbf{u} \cdot \nabla c_- = D_- \nabla^2 c_- - \frac{Fq}{RT} D_- \nabla \cdot (c_- \nabla \phi). \tag{2.8}$$

Here F is Faraday's constant, R is the Gas constant and T is absolute temperature. (Approximate physical data for these constants and others can be found at the end of this Chapter).

The first terms on the right hand sides of (2.7) and (2.8) represent the Fickian diffusion due to concentration gradients in the solution. The second terms give the electrodiffusion due to the migration of charged species in an external electric field of

a potential ϕ. The electrical potential is related to the ionic distribution through the Poisson equation

$$\nabla^2\phi = -\frac{4\pi Fq}{\epsilon_p}(c_+ - c_-), \tag{2.9}$$

where ϵ_p is the solution permittivity.

Equations (2.7), (2.8) and (2.9) form a coupled system of linear partial differential equations for three unknown functions: the concentration of surface-active cations $c_+(\mathbf{x}, t)$, the concentration of counterions $c_-(\mathbf{x}, t)$ and the potential $\phi(\mathbf{x}, t)$. We write Γ for the surface concentration of the cations (notice no subscript as only the positively charged cations are located at the surface), and let Γ_{sat} be the saturated surface concentration which is the largest concentration that the surface can sustain. We can formulate a relationship between the rate of change of the surface concentration of cations and the net flow of these ions to the surface. This introduces a material parameter $\hat{k}$ which is a property of the surfactant-solvent system under consideration, and as a result can only be found using experimental data. Evaluation of this parameter will be discussed later in Chapter 3. The evolution of the surface concentration satisfies

$$\frac{\partial\Gamma}{\partial t} + \nabla\cdot(\mathbf{u}\Gamma) = \frac{1}{\tilde{\tau}c_b}\left[c_{+s}(\Gamma_{sat} - \Gamma) - \hat{k}\Gamma\right], \tag{2.10}$$

where we introduce c_{+s} for the subsurface bulk concentration of cations

$$c_{+s}(x, t) = c_+(x, 0, t),$$

$\tilde{\tau}$ is an adsorption time scale, and c_b is the bulk concentration of surfactant, assumed constant. To obtain $c_\pm$, Γ and ϕ we require suitable initial and boundary conditions for our system.

We choose the following initial conditions

$$c_+(\mathbf{x}, 0) = c_b, \quad c_-(\mathbf{x}, 0) = c_b, \quad \Gamma(x, 0) = 0. \tag{2.11}$$

We also assume that the electrical potential is zero and bulk concentrations of the cations and anions are uniform far from the surface, i.e.

$$\phi \to 0 \quad \text{as } y \to -\infty, \tag{2.12}$$

$$c_+ \to c_b, \quad c_- \to c_b \quad \text{as } y \to -\infty. \tag{2.13}$$

At the free surface, we equate the diffusive flux of cations to the surface with the advection of these ions along the surface, we obtain the condition

$$-D_+\left(\frac{\partial c_+}{\partial y} + \frac{Fq}{RT}c_+\frac{\partial\phi}{\partial y}\right) = \frac{\partial\Gamma}{\partial t} + \nabla\cdot(\mathbf{u}\Gamma) \quad \text{on } y = 0. \tag{2.14}$$

Since there is no flow of the counterions to the surface, by the same argument as above we obtain the condition

$$D_- \left(\frac{\partial c_-}{\partial y} - \frac{Fq}{RT} c_- \frac{\partial \phi}{\partial y} \right) = 0 \quad \text{on } y = 0. \tag{2.15}$$

As previously mentioned, we are considering an ionic model in which only the positively charged cations are adsorbed onto the surface where they reside in a monolayer with a uniform surface concentration. Since we assume that a Stern layer exists at the free surface, the overall electrical potential is reduced. This is achieved by a number of anions attaching themselves to this two-dimensional surface charge layer. The exact percentage of surface cations which are not neutralised in this way and hence can contribute to the electrical potential is currently unknown, yet we may express it as a parameter, the *Stern number* S_T, which we will evaluate later. In other words, S_T is the apparent degree of dissociation (ionisation) of the adsorbed surfactant molecules that represents the portion of the adsorbed surfactant molecules, whose counterions (anions) belong to the diffuse part of the electrical double layer.

Then the electroneutrality condition for the solution as a whole yields the condition

$$\int_{-\infty}^{0} (c_+ - c_-) dy + S_T \Gamma = 0. \tag{2.16}$$

The final condition relates the surface tension γ to the surface concentration of cations Γ by thermodynamic equilibrium (see Adamson [3]) to give the *Frumkin equation*

$$\gamma - \gamma_w = RT\Gamma_{sat} \log \left(1 - \frac{\Gamma}{\Gamma_{sat}} \right), \tag{2.17}$$

where γ_w is the surface tension of water.

2.3 Physical Data

Now that all of the parameters we shall need in our analysis have been introduced, it is appropriate to list their values before any actual theoretical development can be undertaken. Approximate physical data for these parameters are as follows (see Breward *et al.* [7], and Bleaney and Bleaney [6])

$$\begin{aligned} a &\approx 4 \times 10^{-2}\,\text{m}, \\ U_p &\approx 3 \times 10^{-3}\,\text{m s}^{-1}, \\ \rho &\approx 10^{3}\,\text{kg m}^{-3}, \end{aligned}$$

$$
\begin{aligned}
\mu &\approx 10^{-3}\,\mathrm{kg\ m^{-1}\ s^{-1}}, \\
c_b &\approx 0.5\,\mathrm{mol\ m^{-3}}, \\
D_{\pm} &\approx 5 \times 10^{-10}\,\mathrm{m^2\ s^{-1}}, \\
\Gamma_{sat} &\approx 4 \times 10^{-6}\,\mathrm{mol\ m^{-2}}, \\
\gamma_w &\approx 7 \times 10^{-2}\,\mathrm{N\ m^{-1}}, \\
F &\approx 9.6 \times 10^{4}\,\mathrm{C\ mol^{-1}}, \\
RT &\approx 2500\,\mathrm{J\ mol^{-1}} \quad \text{at room temperature.}
\end{aligned}
$$

From here onwards we assume that the diffusivities of the two ionic species are the same, so that we write $D_{\pm} = D$ for the diffusion coefficients of the cations and anions.

The solution permittivity ϵ_p is determined by the relation

$$
\begin{aligned}
\epsilon_p &= \epsilon\epsilon_0 \\
&\approx (81) \times (8.9 \times 10^{-12})\,\mathrm{C^2\ J^{-1}\ m^{-1}} \\
&\approx 7.17 \times 10^{-10}\,\mathrm{C^2\ J^{-1}\ m^{-1}},
\end{aligned}
$$

where ϵ is the relative permittivity of water, and ϵ_0 is the permittivity of the vacuum. The valence q is unitary and is dimensionless. A method for calculating $\hat{k}$ will be discussed in Chapter 3.

Tackling the equations presented above directly without any aforethought is likely to be a fruitless venture as we are dealing with a set of three coupled partial differential equations together with an equally complicated set of initial and boundary conditions. The natural procedure, then, is to work through the above problem systematically, breaking it down into manageable, comprehensive parts which should, in turn, throw some light onto the overall problem.

Chapter 3

The static, steady-state problem

We now go on to assess the ionic model we have developed for the surfactant dynamics by considering the simplest ionic case: the static steady-state problem. In the absence of any motion in the x-direction we may safely assume that all the surfactant dynamics take place in the y-direction (i.e. perpendicular to the surface).

Equations (2.7), (2.8) and (2.9) have now become

$$\frac{d^2c_\pm}{dy^2} \pm \frac{Fq}{RT}\frac{d}{dy}\left(c_\pm \frac{d\phi}{dy}\right) = 0, \tag{3.1}$$

$$\frac{d^2\phi}{dy^2} = -\frac{4\pi Fq}{\epsilon_p}(c_+ - c_-), \tag{3.2}$$

while the corresponding boundary conditions are as follows

$$\phi \to 0, \quad c_\pm \to c_b \quad \text{as } y \to -\infty, \tag{3.3}$$

$$\frac{dc_\pm}{dy} \pm \frac{Fq}{RT}c_\pm \frac{d\phi}{dy} = 0 \quad \text{on } y = 0, \tag{3.4}$$

and, for convenience in our later calculations, we assign a value of ϕ_0 for the electrical potential on the surface. With the advection term eliminated, condition (2.10) can be rearranged to give the *Langmuir isotherm*

$$\Gamma = \frac{\Gamma_{sat}c_{+s}}{\hat{k} + c_{+s}}. \tag{3.5}$$

Furthermore, we may rewrite condition (2.16) by substituting from (3.2) and simplifying to find

$$\int_{-\infty}^{0} \frac{d^2\phi}{dy^2}dy = S_T\frac{4\pi Fq}{\epsilon_p}\Gamma \quad \text{on } y = 0.$$

Integrating the left hand side and using the fact that $\frac{d\phi}{dy} \to 0$ as $y \to -\infty$ (a result of condition (3.3)) we get

$$\frac{d\phi}{dy} = \frac{4\pi Fq}{\epsilon_p} S_T \Gamma \quad \text{on } y = 0. \tag{3.6}$$

The next step of our analysis is to non-dimensionalise our system of equations and boundary conditions. This is done by introducing an arbitrary length scale L and scaling our variables as follows

$$\begin{aligned} y &= L y^*, \\ c_\pm &= c_b c_\pm^*, \\ \Gamma &= \Gamma_{sat} \Gamma^*, \\ \text{and we choose} \quad \phi &= \frac{RT}{Fq} \phi^*, \end{aligned}$$

where $RT/Fq \approx 2.6 \times 10^{-2}$ J C^{-1}.

Dropping the stars, this gives the following set of non-dimensional equations, and initial and boundary conditions

$$\frac{d^2 c_\pm}{dy^2} \pm \frac{d}{dy}\left(c_\pm \frac{d\phi}{dy} \right) = 0, \tag{3.7}$$

$$\omega_1^2 \frac{d^2\phi}{dy^2} = -(c_+ - c_-), \tag{3.8}$$

$$\phi \to 0, \quad c_\pm \to 1 \quad \text{as } y \to -\infty, \tag{3.9}$$

$$\frac{dc_\pm}{dy} \pm c_\pm \frac{d\phi}{dy} = 0 \quad \text{on } y = 0, \tag{3.10}$$

$$\Gamma = \frac{c_{+s}}{\hat{\beta} + c_{+s}}, \tag{3.11}$$

$$\omega_2^2 \frac{d\phi}{dy} = S_T \Gamma \quad \text{on } y = 0. \tag{3.12}$$

Here we have introduced the constants $\hat{\beta}$, ω_1 and ω_2 where

$$\hat{\beta} = \frac{\hat{k}}{c_b}, \tag{3.13}$$

$$\omega_1^2 = \frac{RT\epsilon_p}{4\pi F^2 q^2 c_b L^2}, \tag{3.14}$$

$$\omega_2^2 = \frac{RT\epsilon_p}{4\pi F^2 q^2 L \Gamma_{sat}}. \tag{3.15}$$

We choose $L = L_{Elec}$ such that $\omega_1^2 = 1$. Then L is the lengthscale over which electrical effects occur. This gives us the following values

$$L = L_{Elec} \approx 5.6 \times 10^{-9}\,\mathrm{m}, \tag{3.16}$$

$$\omega_2 = \omega_{Elec} \approx 2.6 \times 10^{-2}. \tag{3.17}$$

Integrating (3.7) twice with respect to y and applying conditions (3.10) and (3.9) in turn, we acquire the following direct relationship between the bulk concentrations of cations/anions and the electrical potential

$$c_{\pm} = \exp(\mp\phi). \tag{3.18}$$

We may now substitute this expression into (3.8) and integrate once with respect to y, applying condition (3.9), to give

$$\frac{d\phi}{dy} = 2\sqrt{2}\,\sinh\left(\frac{\phi}{2}\right). \tag{3.19}$$

Integrating this expression with respect to y and using $\phi = \phi_0$ on $y = 0$, we are left with the equation

$$\tanh\left(\frac{\phi}{4}\right) = \tanh\left(\frac{\phi_0}{4}\right)\exp(\sqrt{2}\,y). \tag{3.20}$$

Substituting (3.18) into the Langmuir isotherm (3.5), and (3.19) into (3.12) we gain the important expressions

$$\Gamma = \frac{e^{-\phi_0}}{\hat{\beta} + e^{-\phi_0}}, \tag{3.21}$$

$$\frac{S_T}{\omega_{Elec}^2}\Gamma = 2\sqrt{2}\,\sinh\left(\frac{\phi_0}{2}\right). \tag{3.22}$$

Although ω_{Elec}^2 is of the order of magnitude 10^{-4}, we keep this term in (3.22) because we presume that S_T is of order ω_{Elec}^2. The combination of (3.21) and (3.22) then gives a useful relation, since they allow the calculation of the values of the surface surfactant concentration Γ, and the surface potential ϕ_0, at a given surfactant bulk concentration c_b and for a chosen value of S_T.

The next step in our analysis is to determine a way of calculating values of $\hat{\beta}$ for our system. Let us briefly go back to dimensional parameters for one moment. As previously mentioned, the model presented by Breward *et al.* [7] was nonionic and the value of the nonionic equivalent of $\hat{k}$, k, was found by fitting the nonionic Langmuir isotherm (which is of the same form as (3.5)) with experimentally measured values of Γ versus $c_b\,(=\ c_s)$ [1], since the measurements were taken under static conditions

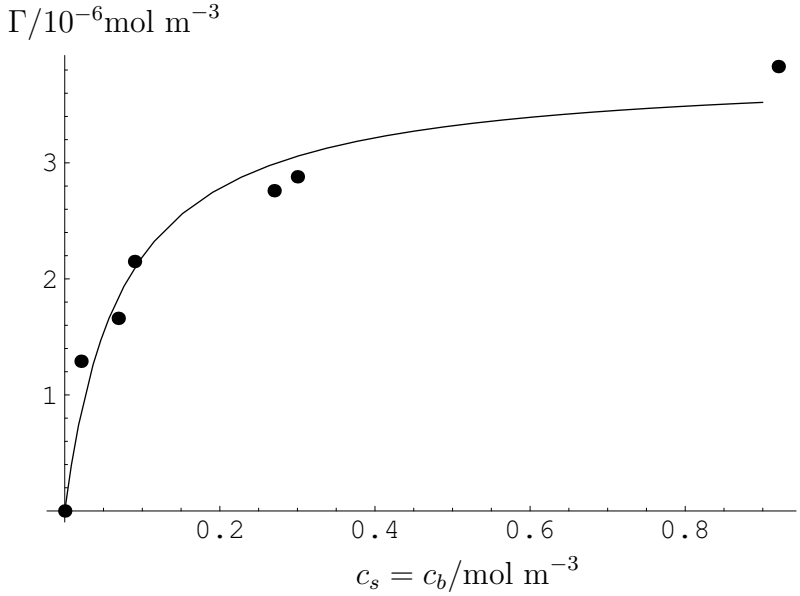


Figure 3.1: Experimental static values of surface concentration Γ and subsurface bulk concentration c_s, fitted with a Langmuir isotherm $\Gamma = \Gamma_{sat}\, c_s/(k + c_s)$.

(see Figure 3.1). We note in passing that the best fit shown is not particularly good. This method may also be used to determine the value of $\hat{k}$ in the ionic model. In the nonionic model, the above method obtains the values $\Gamma_{sat} \approx 4 \times 10^{-6}\,\mathrm{mol\ m^{-2}}$ and $k \approx 0.08\,\mathrm{mol\ m^{-3}}$. When non-dimensionalised, the nonionic Langmuir isotherm reduces to the form

$$\Gamma = \frac{c_s}{\beta + c_s}, \tag{3.23}$$

where $\beta = k/c_b \approx 0.16$ is known. In the nonionic static problem, where $c_s = 1$, (3.23) reduces to

$$\Gamma = \frac{1}{\beta + 1}. \tag{3.24}$$

Thus we have a method for calculating our ionic value of $\hat{\beta}$: by equating our static ionic Langmuir isotherm (3.5) with (3.24) we get a direct relationship between $\hat{\beta}$ and β by the following steps

$$\frac{e^{-\phi_0}}{\hat{\beta} + e^{-\phi_0}} = \frac{1}{\beta + 1},$$

which then gives us

$$\hat{\beta} = \beta e^{-\phi_0}. \tag{3.25}$$

We see that $\hat{\beta}$ is dependent upon ϕ_0 which, in turn, will vary for different values of

[1]Notice no "+" subscript as the model in Breward *et al.* [7] was nonionic

S_T and ω_{Elec}. (3.22) gives us a direct relationship for ϕ_0, namely

$$2\sqrt{2}\,\omega_{Elec}^2 \sinh\left(\frac{\phi_0}{2}\right) = \frac{S_T}{\beta+1}, \tag{3.26}$$

which we may rearrange to give

$$\phi_0 = 2\sinh^{-1}\left(\frac{S_T}{2\sqrt{2}\,\omega_{Elec}^2(\beta+1)}\right),$$

where the constant $1/2\sqrt{2}\,\omega_{Elec}^2(\beta+1) \approx 438$.

Thus for different values of S_T we obtain different values of ϕ_0. This is consistent with the theory of this system: different values of S_T reflect different degrees of ionisation of the surfactant molecules on the surface and hence should affect the electrical potential found at the surface ϕ_0. So by calculating the different values of ϕ_0 and the corresponding values of the cationic/anionic subsurface concentrations, c_{+s} and c_{-s}, for varying S_T we can make a reasonable guess at the composition of the Stern layer.

Let us consider a value of $S_T = 1$. Although this violates the condition $S_T = O(\omega_{Elec}^2)$ we do it anyway, for reasons later explained in Chapter 4. This value of S_T represents the situation where none of the surface cations have been neutralised by the anions; so that, effectively, there is no Stern layer present. We then find that we run into difficulties in the subsurface, since we find that

$$\begin{aligned} \phi_0 &\approx 350\,\text{mV}, \\ c_{+s} &\approx 7.1 \times 10^{-7}\,\text{mol m}^{-3}, \\ c_{-s} &\approx 3.5 \times 10^{5}\,\text{mol m}^{-3}. \end{aligned}$$

The corresponding value for $\hat{\beta}$ is found to be approximately 2.3×10^{-7}.

The values for ϕ_0 and c_{+s} are acceptible as they are within the physical and chemical bounds of the system, given a bulk concentration of $0.5\,\text{mol m}^{-3}$. The value for c_{-s}, however, causes some concern since such a high concentration of anions in the subsurface is chemically unlikely, especially at bulk concentrations below the CMC. We hope, therefore, that the inclusion of a Stern layer will modify these results, making them more physically realistic.

We take a value of $S_T = O(\omega_{Diff})$, where ω_{Diff} is the diffusive equivalent to ω_{Elec}, whose value is given in Section 4.2. Then $S_T = 7.3 \times 10^{-4}$ and represents a situation

where only 0.073% of the surface cations contribute to the surface charge as 99.9% of them have been neutralised. We then obtain the values

$$\begin{aligned} \phi_0 &\approx 15.6\,\text{mV}, \\ c_{+s} &\approx 0.27\,\text{mol m}^{-3}, \\ c_{-s} &\approx 0.91\,\text{mol m}^{-3}. \end{aligned}$$

The corresponding value for $\hat{\beta}$ is found to be approximately 0.09.

Furthermore, let us also take a value of $S_T = O(\omega_{Diff}^2)$ (see end of Chapter 4), i.e. $S_T = 5.3 \times 10^{-7}$. We then get the values

$$\begin{aligned} \phi_0 &\approx 0.012\,\text{mV}, \\ c_{+s} &\approx 0.5\,\text{mol m}^{-3}, \\ c_{-s} &\approx 0.5\,\text{mol m}^{-3}. \end{aligned}$$

The corresponding value for $\hat{\beta}$ is found to be approximately 0.16.

A typical plot for ϕ and c_{+s}, given varying values of S_T, can be seen in Figures 3.2 to 3.4. Examining Figures 3.2 to 3.4, we see that for each valuer of S_T there is a gentle

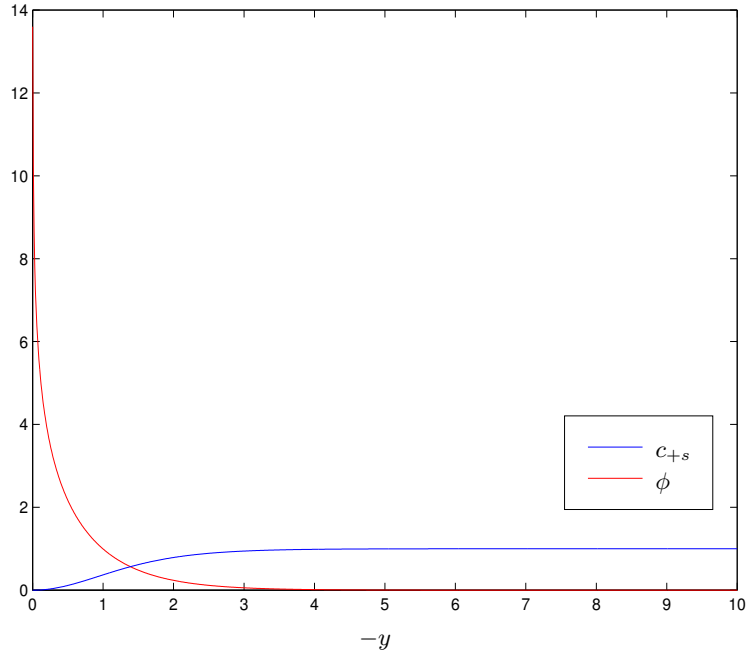


Figure 3.2: Electrical potential ϕ and cationic subsurface concentration c_{+s} versus depth ($S_T = 1$). c_{-s} is not shown because it is too large at the free surface.

rise in the electrical potential from zero at depth, to its surface value. Meanwhile,

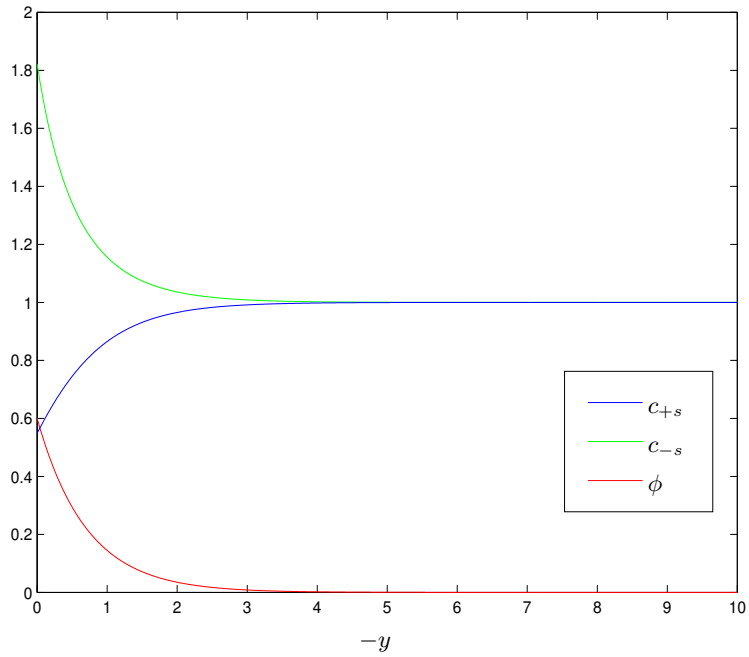


Figure 3.3: Electrical potential ϕ, cationic subsurface concentration c_{+s} and anionic subsurface concentration c_{-s} versus depth ($S_T = \omega_{Diff}$).

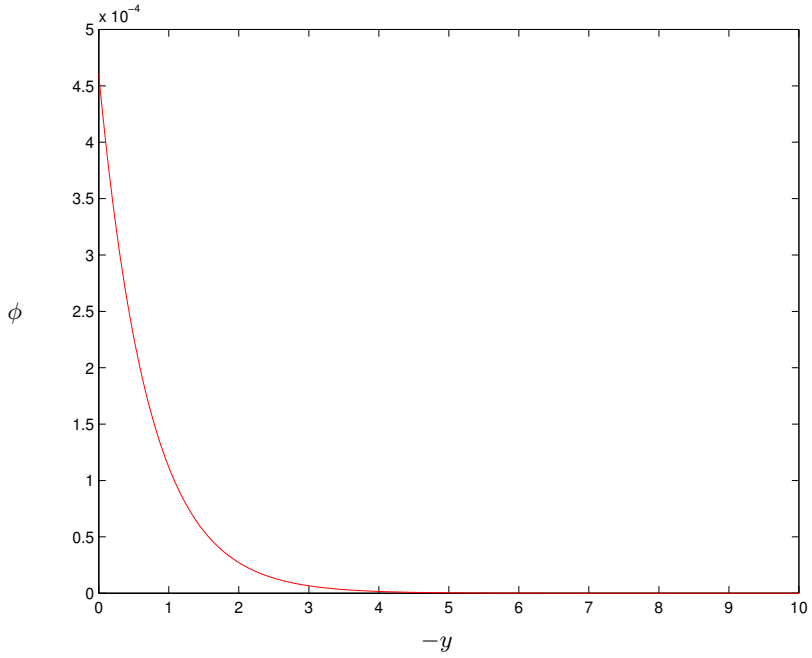


Figure 3.4: Electrical potential ϕ versus depth ($S_T = \omega^2_{Diff}$). c_{+S} and c_{-s} not shown as they are approximately 1 throughout.

the subsurface concentration of cations decreases from its bulk value, 1, at depth to zero at the surface. The subsurface concentration of anions however increases from its bulk value, 1, at depth to a larger value on the surface. As S_T gets smaller (i.e. going from Figure 3.2 to 3.4), the surface electrical potential ϕ_0 is reduced as the number of unbound free surface cations is lowered. Then the differences between the subsurface concentrations of cations and anions and their bulk concentrations is significantly reduced (going from Figures 3.2 to 3.4) as the repelling force of the surface electrical potential is lower. This is further reflected in our calculated values: we see that, as our value of S_T tends to zero , the surface electrical potential clearly decreases and the subsurface concentrations of the cations and anions tend towards the bulk concentration value. Consequently, we see a reduction in the concentration gradient from the bulk solution to the subsurface region and this will prove to have significant implications when we come to look at the time-dependent problem.

In this chapter, we have presented a method for calculating the values of ϕ_0 for each chosen value of S_T. This then allows us to calculate the value of $\hat{\beta}$ using relation (3.25) which, in turn, is used to calculate the value of the surface concentration Γ using the altered Langmuir isotherm

$$\Gamma = \frac{c_{+s}}{\beta e^{-\phi_0} + c_{+s}}. \tag{3.27}$$

The values of $\hat{\beta}$ and ϕ_0 calculated here will be required at the end of Chapter 4.

Chapter 4

The static, time-dependent problem

We go on now to look at the problem of the static, time-dependent surfactant adsorption at an initially "clean" (i.e. surfactant free) surface. We consider this in two parts: Section 4.1 examines the nonionic problem; Section 4.2 examines the ionic problem. The latter is likely to involve the analysis of an electrical boundary layer whose solution far from the surface will be equivalent to the nonionic case.

4.1 The nonionic case

As with the steady-state problem presented in Chapter 3, under static conditions there are no variations of the dependent variables in the x-direction. Equations (2.7), (2.8) have now become

$$\frac{\partial c}{\partial t} = D\,\frac{\partial^2 c}{\partial y^2}, \tag{4.1}$$

and (2.10) reads

$$\frac{\partial \Gamma}{\partial t} = \frac{1}{\tilde{\tau} c_b}\left[c_s(\Gamma_{sat} - \Gamma) - \hat{k}\Gamma\right]. \tag{4.2}$$

(notice no "$\pm$" subscripts as we are considering the nonionic case). There is no equivalent to (2.9) since there is no electrical potential in our system. The corresponding initial and boundary conditions are as follows

$$c(y,0) = c_b, \quad \Gamma(0) = 0, \tag{4.3}$$

$$c \to c_b \quad \text{as } y \to -\infty, \tag{4.4}$$

$$-D\frac{\partial c}{\partial y} = \frac{\partial \Gamma}{\partial t} \quad \text{on } y = 0. \tag{4.5}$$

As before, the next step of our analysis is to non-dimensionalise our system of equations and their initial and boundary conditions. Introducing an arbitrary length scale L and scaling our variables as follows:

$$\begin{aligned} y &= Ly^*, \\ c &= c_b c^*, \\ \Gamma &= \Gamma_{sat}\Gamma^*, \\ t &= \tau t^*. \end{aligned}$$

We choose L and τ to balance terms in (4.1) and (4.5), thus

$$\frac{\tau D}{L^2} = 1, \quad \frac{c_b \tau D}{\Gamma_{sat} L} = 1,$$

which then gives us values of

$$L = L_{Diff} \approx 7.6 \times 10^{-6}\,\mathrm{m}, \quad \tau \approx 0.12\,\mathrm{s}, \tag{4.6}$$

where L_{Diff} is the diffusive length scale. On dropping the stars, this gives the following set of non-dimensional equations, and initial and boundary conditions

$$\frac{\partial c}{\partial t} = \frac{\partial^2 c}{\partial t^2}, \tag{4.7}$$

$$\frac{\partial \Gamma}{\partial t} = T\left[c_{+s}(1-\Gamma) - \hat{\beta}\,\Gamma\right], \tag{4.8}$$

$$c(y,0) = 1, \tag{4.9}$$

$$\Gamma(0) = 0, \tag{4.10}$$

$$c \to 1 \quad \text{as } y \to -\infty, \tag{4.11}$$

$$-\frac{\partial c}{\partial y} = \frac{\partial \Gamma}{\partial t} \quad \text{on } y = 0, \tag{4.12}$$

where we have introduced $T = \tau/\hat{\tau}$ which is the ratio of the diffusive time scale τ to the adsorption time scale $\hat{\tau}$, and $\hat{\beta}$ is the same as before.

We may solve (4.7) with conditions (4.9) and (4.11) by a Green's fuction method (see Ockendon, Howison, Lacey, and Movchan [18]) to give us

$$c(y,t) = 1 + \frac{1}{2\sqrt{\pi}} \int_0^t \frac{1 - c_s(\tau)}{(t-\tau)^{3/2}}\, y\, \exp\frac{-y^2}{4(t-\tau)}\, d\tau. \tag{4.13}$$

We want to differentiate (4.13) with respect to y and take the limit as $y \to 0$. This involves first splitting the range of integration into $[0, t-\delta] \cap [t-\delta, t]$ (where $\delta << 1$) and considering these two integrals separately

$$c(y,t) = 1 + I_1 + I_2, \tag{4.14}$$

where

$$I_1 = \frac{1}{2\sqrt{\pi}} \int_0^{t-\delta} \frac{1-c_s(\tau)}{(t-\tau)^{3/2}}\, y\, \exp\frac{-y^2}{4(t-\tau)}\, d\tau, \tag{4.15}$$

$$I_2 = \frac{1}{2\sqrt{\pi}} \int_{t-\delta}^{t} \frac{1-c_s(\tau)}{(t-\tau)^{3/2}}\, y\, \exp\frac{-y^2}{4(t-\tau)}\, d\tau. \tag{4.16}$$

We now replace y with $-y$ in our equations. In I_1, we expand for small y and integrate by parts to give us

$$I_1 = y\left\{ \frac{1-c_s(t-\delta)}{\sqrt{\pi\,\delta}} + \frac{1}{\sqrt{\pi}} \int_0^{t-\delta} \frac{c_s'(\tau)}{(t-\tau)^{1/2}}\, d\tau \right\} + O(y^3). \tag{4.17}$$

Similarly, I_2 is calculated by performing the substitution $\tau = t - y^2/4r$ in (4.16) and then expanding for small y. This gives

$$I_2 = 1 - c_s - y\left\{ \frac{1-c_s(t)}{\sqrt{\pi\,\delta}} - \frac{\sqrt{\delta}}{\sqrt{\pi}} c_s'(t) \right\} + O(y^2). \tag{4.18}$$

We see that straight substitution of (4.17) and (4.18) into (4.14), in the limit $y \to 0$, gives c_s thus confirming showing that (4.13) works. Meanwhile, adding (4.17) and (4.18), differentiating with repect to y, and taking the limit $y \to 0$ gives the expression

$$\frac{\partial c}{\partial y}(0,t) = -\frac{1}{\sqrt{\pi}} \int_0^t \frac{c_s'(\tau)}{(t-\tau)^{1/2}}\, d\tau, \tag{4.19}$$

in the limit $\delta \to 0$. Integrating (4.19) by parts and equating with (4.12) give us

$$\frac{\partial \Gamma}{\partial t} = \frac{1}{\sqrt{\pi}} \frac{d}{dt} \int_0^t \frac{1-c_s(\tau)}{(t-\tau)^{1/2}}\, d\tau, \tag{4.20}$$

which, when integrated reduces to

$$\Gamma = \frac{1}{\sqrt{\pi}} \int_0^t \frac{1-c_s(\tau)}{(t-\tau)^{1/2}}\, d\tau, \tag{4.21}$$

where the constant of integration is set to zero by applying condition (4.10). We now have two simultaneous equations in terms of c_s and Γ

$$\frac{d\Gamma}{dt} = T\left[c_s(1-\Gamma) - \hat{\beta}\Gamma\right] = \frac{1}{\sqrt{\pi}} \frac{d}{dt} \int_0^t \frac{(1-c_s)}{\sqrt{t-\tau}}\, d\tau,$$

with the conditions $\Gamma = 0$, $c_s = 1$ at $t = 0$. We define $c_s = 1 - \psi$ so that the problem becomes

$$\frac{d\Gamma}{dt} = T\left[(1-\psi)(1-\Gamma) - \hat{\beta}\Gamma\right] = \frac{1}{\sqrt{\pi}}\frac{d}{dt}\int_0^t \frac{\psi(\tau)}{\sqrt{t-\tau}}\,d\tau,$$

with $\Gamma = \psi = 0$ at $t = 0$. Thus, rewriting (4.21),

$$\Gamma(t) = \frac{1}{\sqrt{\pi}}\int_0^t \frac{\psi(\tau)}{\sqrt{t-\tau}}\,d\tau.$$

Now, we want to invert this equation so that we have an expression for ψ in terms of Γ. This can be done by considering the Laplace transform (see Priestley [19]) of Γ and writing this as the convolution of ψ and some function g

$$\bar{\Gamma}(p) = \frac{1}{\sqrt{\pi}}\,\bar{\psi}(p)\,\bar{g}(p),$$

where $g(t) = 1/\sqrt{t}$. Then $\bar{g}(p) = \sqrt{\pi/p}$ and we may rewrite the above as

$$\bar{\psi}(p) = \sqrt{p}\,\bar{\Gamma}(p) = p\left(\frac{\bar{\Gamma}(p)}{\sqrt{p}}\right),$$

$$\Rightarrow \bar{\psi}(p) = p\,\bar{f}(p),$$

where $\bar{f}(p) = \bar{\Gamma}(p)/\sqrt{p}$. Note that this means that $\bar{\psi}$ is then the Laplace transform of f', so that this reduces to

$$\psi(t) = f'(t),$$

where

$$f(t) = \frac{1}{\sqrt{\pi}}\int_0^t \frac{\Gamma(\tau)}{(t-\tau)^{1/2}}d\tau,$$

by the convolution theorem. We then have

$$\psi(t) = \frac{1}{\sqrt{\pi}}\frac{d}{dt}\int_0^t \frac{\Gamma(\tau)}{(t-\tau)^{1/2}}d\tau.$$

Then integrating by parts and using $\Gamma(0) = 0$ we obtain

$$\psi(t) = \frac{1}{\sqrt{\pi}}\int_0^t \frac{\Gamma'(\tau)}{(t-\tau)^{1/2}}d\tau. \tag{4.22}$$

Substituting for $\Gamma'(t)$ we are then left with the two simultaneous Abel integral equations

$$\psi(t) = \frac{T}{\sqrt{\pi}}\int_0^t \frac{\left[(1-\psi(\tau))(1-\Gamma(\tau)) - \hat{\beta}\Gamma(\tau)\right]}{\sqrt{t-\tau}}\,d\tau, \tag{4.23}$$

$$\Gamma(t) = \frac{1}{\sqrt{\pi}}\int_0^t \frac{\psi(\tau)}{\sqrt{t-\tau}}\,d\tau. \tag{4.24}$$

We have two possible methods for calculating c and Γ: (1) solve the system of Abel equations (4.23), (4.24) to get ψ, Γ and hence find c_s which then enables us to get c from (4.13); (2) solve the system (4.7) to (4.12) numerically to determine Γ and c. We use method (1) in 4.1.1 and method (2) in 4.1.2 for c and Γ. Note that for this nonionic case $\hat{\beta} = \beta = 0.16$.

4.1.1 Numerical scheme for the Abel equations

We wish to solve the two Abel equations (4.23) and (4.24) simultaneously using a suitable numerical scheme. This can be done by dividing $(0, t)$ into n uniform intervals $I_j = (j\Delta t, (j+1)\Delta t)$ for $j = 0, \ldots, (n-1)$, where $t = n\Delta t$. Then the two integral equations (4.23) and (4.24) may be written in the form

$$\Gamma(n\Delta t) = \frac{1}{\sqrt{\pi}} \sum_{j=0}^{n-1} \int_{I_j} \frac{\psi(\tau)}{\sqrt{n\Delta t - \tau}}\, d\tau, \tag{4.25}$$

$$\psi(n\Delta t) = \frac{T}{\sqrt{\pi}} \sum_{j=0}^{n-1} \int_{I_j} \frac{[(1-\psi(\tau))(1-\Gamma(\tau)) - \beta\Gamma(\tau)]}{\sqrt{n\Delta t - \tau}}\, d\tau. \tag{4.26}$$

If the values at the grid points are denoted by

$$\psi(j\Delta t) = \psi_j, \quad \Gamma(j\Delta t) = \Gamma_j, \tag{4.27}$$

then our integrals in (4.25) and (4.26) are evaluated by approximating ψ and Γ as piecewise linear functions in each interval

$$\psi(\tau) \approx \psi_j + \left(\frac{\tau}{\Delta t} - j\right)(\psi_{j+1} - \psi_j) \quad \text{in } I_j, \tag{4.28}$$

$$\Gamma(\tau) \approx \Gamma_j + \left(\frac{\tau}{\Delta t} - j\right)(\Gamma_{j+1} - \Gamma_j) \quad \text{in } I_j. \tag{4.29}$$

We may then explicitly evaluate the integrals in (4.25) and (4.26) by substituting in our functions (4.28) and (4.29) and integrating by parts, giving us

$$\begin{aligned} \Gamma_n = {} & \frac{2\sqrt{\Delta t}}{3\sqrt{\pi}} \sum_{j=0}^{n-1} \Big\{ \sqrt{n-j-1}\,[2(n-j-1)\psi_j - (2n-2j+1)\psi_{j+1}] \\ & + \sqrt{n-j}\,[2(n-j)\psi_{j+1} - (2n-2j-3)\psi_j] \Big\}, \end{aligned} \tag{4.30}$$

$$\begin{aligned} \psi_n = {} & \frac{T\sqrt{\Delta t}}{15\sqrt{\pi}} \sum_{j=0}^{n-1} \Big\{ \sqrt{n-j-1}\,[-30 - 20(n-j-1)(\psi_j + (1+\beta)\Gamma_j) \\ & + 10(2n-2j+1)(\psi_{j+1} + (1+\beta)\Gamma_{j+1}) - 16(n-j-1)^2\psi_j\Gamma_j \end{aligned}$$

$$
\begin{aligned}
&-(16(n-j)^2+8n-8j+6)\psi_{j+1}\Gamma_{j+1}\\
&+4(n-j-1)(4n-4j+1)(\psi_j\Gamma_{j+1}+\psi_{j+1}\Gamma_j)]\\
&+\sqrt{n-j}\,[30+10(2n-2j-3)(\psi_j+(1+\beta)\Gamma_j)\\
&-20(n-j)(\psi_{j+1}+(1+\beta)\Gamma_{j+1})\\
&+(16(n-j)^2-40n+40j+30)\psi_j\Gamma_j+16(n-j)^2\psi_{j+1}\Gamma_{j+1}\\
&-4(n-j)(4n-4j-5)(\psi_j\Gamma_{j+1}+\psi_{j+1}\Gamma_j)]\}\,. \qquad (4.31)
\end{aligned}
$$

We start with the initial values $\psi_0=\Gamma_0=0$, and then, for each value of $n=1,2,\ldots$, given $\psi_0,\ldots,\psi_{n-1}$ and $\Gamma_0,\ldots,\Gamma_{n-1}$, (4.30) and (4.31) are two simultaneous nonlinear equations for ψ_n and Γ_n. By grouping together the coefficients of our functions at level n, they may be written in the form

$$
\begin{aligned}
\psi_n &= A+B\psi_n+C\Gamma_n+D\psi_n\Gamma_n, \qquad (4.32)\\
\Gamma_n &= a+b\psi_n, \qquad (4.33)
\end{aligned}
$$

where

$$
\begin{aligned}
a &= \frac{2\sqrt{\Delta t}}{3\sqrt{\pi}}\left[\sum_{j=0}^{n-2}\left\{\sqrt{n-j-1}\,[2(n-j-1)\psi_j-(2n-2j+1)\psi_{j+1}]\right.\right.\\
&\quad \left.\left.+\sqrt{n-j}\,[2(n-j)\psi_{j+1}-(2n-2j-3)\psi_j]\right\}+\psi_{n-1}\right], \qquad (4.34)\\
b &= \frac{4\sqrt{\Delta t}}{3\sqrt{\pi}}, \qquad (4.35)\\
A &= \frac{T\sqrt{\Delta t}}{15\sqrt{\pi}}\left[\sum_{j=0}^{n-2}\left\{\sqrt{n-j-1}\,[-30-20(n-j-1)(\psi_j+(1+\beta)\Gamma_j)\right.\right.\\
&\quad +10(2n-2j+1)(\psi_{j+1}+(1+\beta)\Gamma_{j+1})-16(n-j-1)^2\psi_j\Gamma_j\\
&\quad -(16(n-j)^2+8n-8j+6)\psi_{j+1}\Gamma_{j+1}\\
&\quad +4(n-j-1)(4n-4j+1)(\psi_j\Gamma_{j+1}+\psi_{j+1}\Gamma_j)]\\
&\quad +\sqrt{n-j}\,[30+10(2n-2j-3)(\psi_j+(1+\beta)\Gamma_j)\\
&\quad -20(n-j)(\psi_{j+1}+(1+\beta)\Gamma_{j+1})\\
&\quad +(16(n-j)^2-40n+40j+30)\psi_j\Gamma_j+16(n-j)^2\psi_{j+1}\Gamma_{j+1}\\
&\quad \left.\left.-4(n-j)(4n-4j-5)(\psi_j\Gamma_{j+1}+\psi_{j+1}\Gamma_j)]\right\}\right.\\
&\quad \left.+30-10(\psi_{n-1}+(1+\beta)\Gamma_{n-1})+6\psi_{n-1}\Gamma_{n-1}\right], \qquad (4.36)\\
B &= \frac{T\sqrt{\Delta t}}{15\sqrt{\pi}}\,(-20+4\Gamma_{n-1})\,, \qquad (4.37)\\
C &= \frac{T\sqrt{\Delta t}}{15\sqrt{\pi}}\,(-20(1+\beta)+4\psi_{n-1})\,, \qquad (4.38)
\end{aligned}
$$

$$D = \frac{16T\sqrt{\Delta t}}{15\sqrt{\pi}}. \tag{4.39}$$

So once these six constants have been calculated, ψ_n may be calculated directly from

$$\psi_n = \frac{1 - aD - bC - B - \sqrt{(1 - aD - bC - B)^2 - 4bD(A + aC)}}{2bD}, \tag{4.40}$$

and then Γ_n is found from (4.33).

We solve this sytem using Fortran, and we show how Γ and c_s behave with time for different values of T in Figures 4.1 and 4.2. We show the Γ and c_s behaviour for one of these values of T for a longer period of time in figure 4.3. The Fortran coding for this scheme may be found in Appendix A.

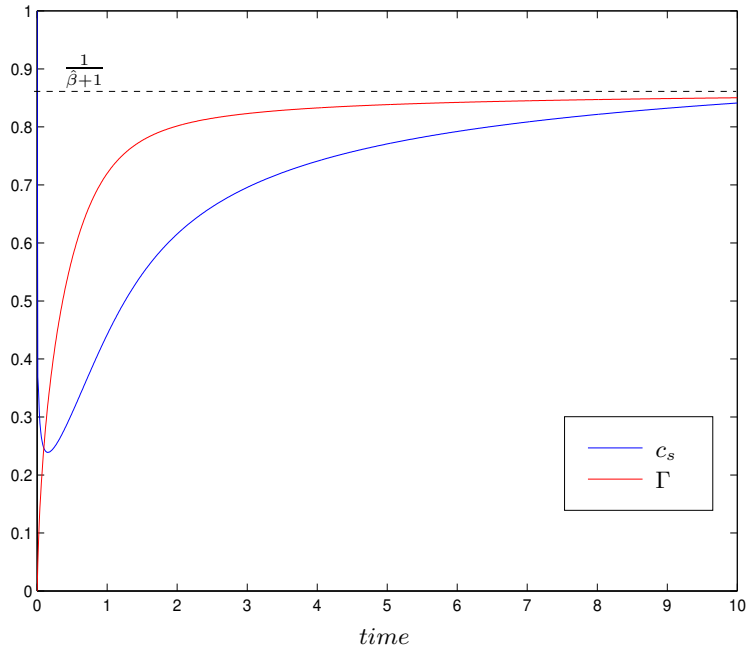


Figure 4.1: Surface concentration Γ and subsurface concentration c_s up to time $t = 10$ ($T = 10$, $\hat{\beta} = \beta = 0.16$).

We postpone the discussion of these results until Section 4.1.3.

4.1.2 Numerical scheme for the diffusion equation

In this section we solve the original problem ((4.7) to (4.12)) directly by applying an implicit central difference scheme. We firstly replace y with $-y$ in the equations (4.7) to (4.12) since we must discretise a positive interval for our scheme. A first-order difference is used to march in the t-direction, such that the problem to be solved at

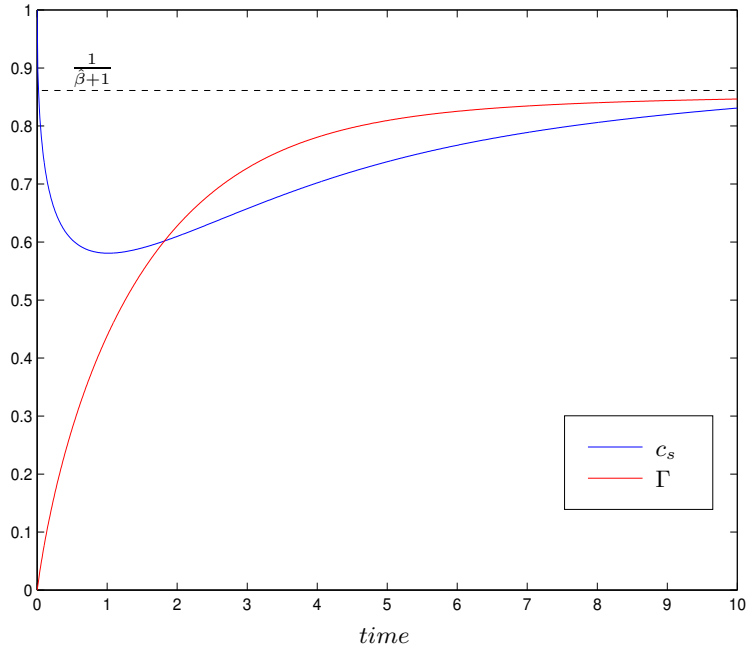


Figure 4.2: Surface concentration Γ and subsurface concentration c_s up to time $t = 10$ ($T = 1$, $\hat{\beta} = \beta = 0.16$).

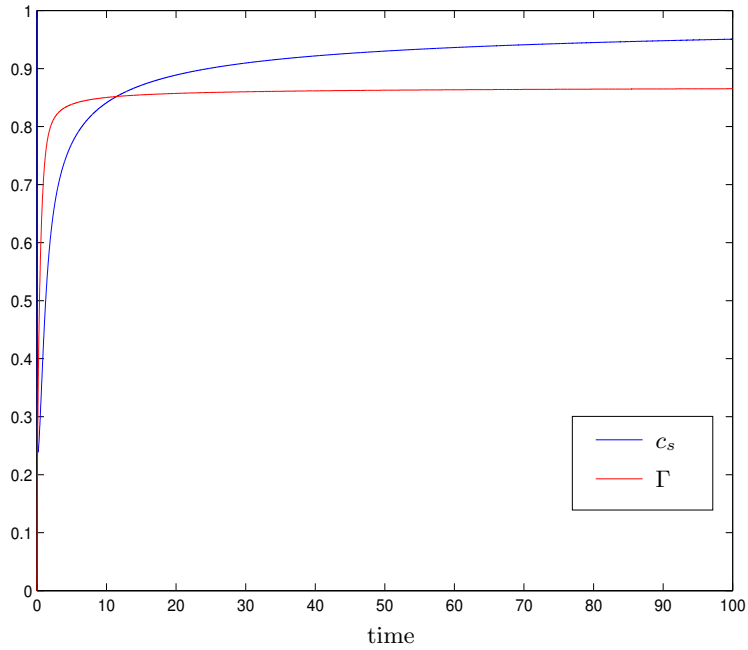


Figure 4.3: Surface concentration Γ and subsurface concentration c_s up to time $t = 100$ ($T = 10$, $\hat{\beta} = \beta = 0.16$).

each new value of t is linear. We divide $(0, t)$ into N uniform intervals of width Δt so that $t_n = n\Delta t$. We truncate at a final depth L_d in the y-direction and discretise the interval $[0, L_d]$ using a uniform mesh: $y_j = j\Delta y$, $\Delta y = L_d/J$ for some integer J. We then have the finite difference scheme: for $j = 1, 2, ..., J-1$ and $n = 1, 2, ..., N-1$

$$\frac{c_j^{n+1} - c_j^n}{\Delta t} = \frac{c_{j+1}^{n+1} - 2c_j^{n+1} + c_{j-1}^{n+1}}{(\Delta y)^2}, \tag{4.41}$$

$$\frac{\Gamma^{n+1} - \Gamma^n}{\Delta t} = T\left[c_0^{n+1}(1 - \Gamma^n) - \beta\Gamma^n\right], \tag{4.42}$$

with the boundary condition

$$\left(\frac{c_0^{n+1} - c_0^{n+1}}{\Delta y}\right) = \frac{\Gamma^{n+1} - \Gamma^n}{\Delta t}, \tag{4.43}$$

and starting with the values $\Gamma^0 = 0$, $c_j^0 = 1$. We also set $c_J^n = 1$ to represent the condition $c \to 1$ as $y \to \infty$.

We solve this system using Matlab and view how c behaves in time and space in Figures 4.4 and 4.6. We also gain the corresponding Γ and c_s profiles in Figures 4.5 and 4.7. Note that we have not reached the steady state by $t = 10$ (see Figure 4.3). Diffusion will (slowly) replenish the subsurface concentration so that $c_s \to 1$ as $t \to \infty$. The Matlab coding for this scheme may be found in Appendix B.

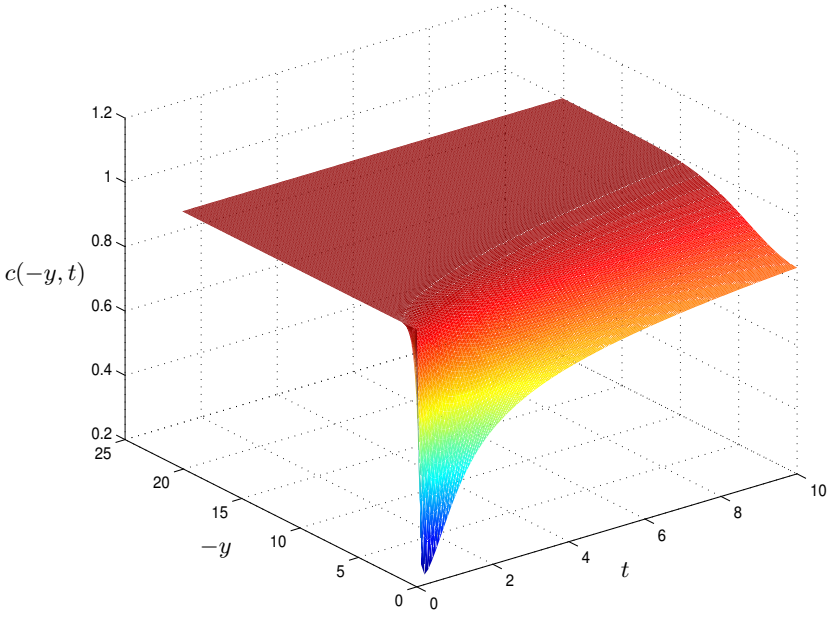


Figure 4.4: Bulk concentration c variation in space and time ($T = 10$, $\hat{\beta} = \beta = 0.16$).

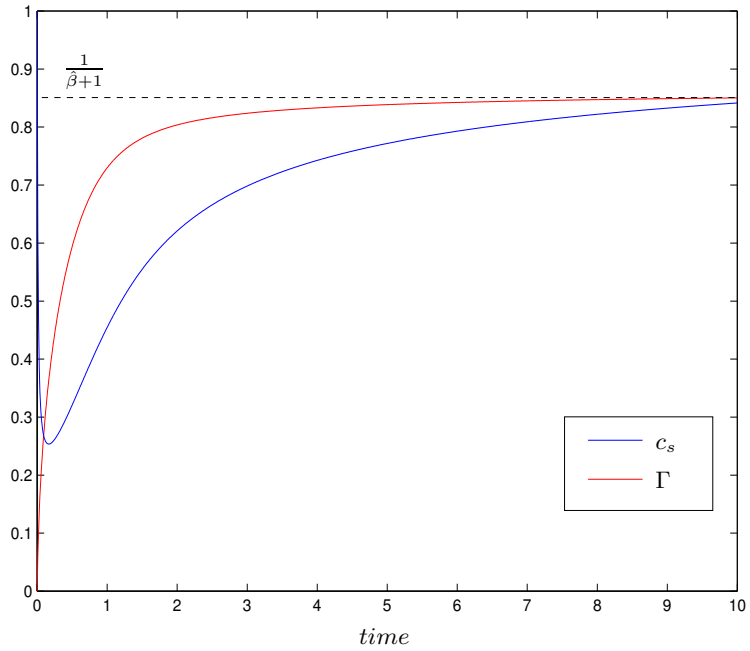


Figure 4.5: Surface concentration Γ and subsurface concentration c_s up to time $t = 10$ ($T = 10$, $\hat{\beta} = \beta = 0.16$).

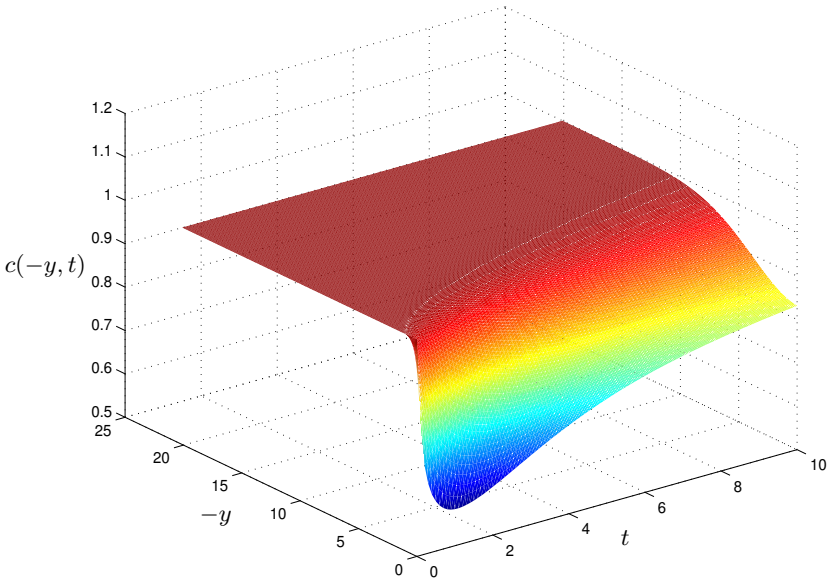


Figure 4.6: Bulk concentration c variation in space and time ($T = 1$, $\hat{\beta} = \beta = 0.16$).

4.1.3 Discussion of results

Comparing Figures 4.1 and 4.2 for the scheme in Section 4.1.1 with Figures 4.5 and 4.7 for the scheme in Section 4.1.2, we see that both numerical methods give exactly the same profiles for Γ and c_s against time, showing that our numerical schemes are well constructed and that our results are of a similar accuracy. The latter scheme also has the added benefit of producing a three dimensional plot which gives us a good idea of how the bulk concentration c is behaving. Now, looking at the c_s profiles alone, we see that it at first decreases, because of adsorption of surfactant at the surface. Diffusion then sets in and surfactant is transported from further below the surface up to replenish the subsurface layer. The levels of surface and subsurface surfactant then grow slowly as the system settles to its steady state as $t \to \infty$. Figure 4.3 indeed shows that c_s tends back to its equilibrium value of c_b (after re-dimensionalising) very slowly. The corresponding value of Γ increases from zero due to the subsurface molecules (remembering this is the nonionic case) adsorbing onto the surface. For greater time we see that Γ tends to its equilibrium value of $1/(\beta + 1)$ which is a direct result of the limit $c_s \to 1$ in the non-dimensional nonionic Langmuir isotherm. Furthermore, by direct comparison of Figures 4.1 and 4.2, we see that by varying T we vary the speeds with which the processes of adsorption and diffusion act on our system. The greater the value of T, the faster Γ tends to its limit $1/(\beta + 1)$, and the more rapid the initial drop of c_s. This can be explained by the fact that an increase in T corresponds to a longer period of time over which it takes diffusion to act and hence replenish c_s, whilst the process of adsorption is more dominant and hence causes Γ to rise quickly. We note that, in both the cases that we have presented, it takes a long time for c_s to reach its equilibrium value.

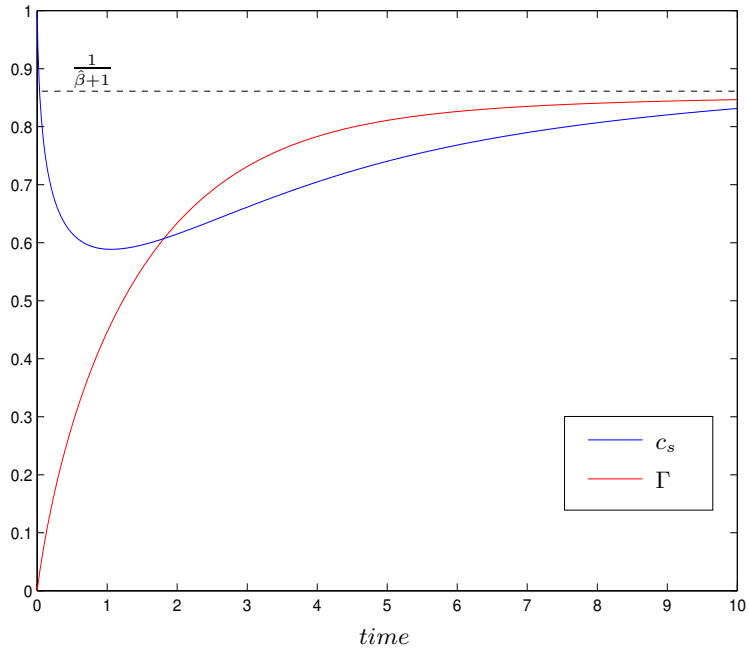


Figure 4.7: Surface concentration Γ and subsurface concentration c_s up to time $t = 10$ ($T = 1$, $\hat{\beta} = \beta = 0.16$).

4.2 The ionic case

We are now in a position to go on and consider the static, time-dependent ionic problem. The equations governing this system are then

$$\frac{\partial c_\pm}{\partial t} = D\frac{\partial^2 c_\pm}{\partial y^2} \pm \frac{Fq}{RT}\frac{\partial}{\partial y}\left(c_\pm \frac{\partial \phi}{\partial y}\right), \tag{4.44}$$

$$\frac{\partial^2 \phi}{\partial y^2} = -\frac{4\pi F q}{\epsilon_p}(c_+ - c_-), \tag{4.45}$$

$$\frac{\partial \Gamma}{\partial t} = \frac{1}{\tilde{\tau} c_b}\left[c_{+s}(\Gamma_{sat} - \Gamma) - \hat{k}\Gamma\right]. \tag{4.46}$$

with the initial and boundary conditions

$$c_\pm(y,0) = c_b, \quad \Gamma(0) = 0, \tag{4.47}$$

$$\phi = \phi_0 \quad \text{on } y = 0, \tag{4.48}$$

$$\phi \to 0 \quad \text{as } y \to -\infty, \tag{4.49}$$

$$c_\pm \to c_b \quad \text{as } y \to -\infty, \tag{4.50}$$

$$-D\left(\frac{\partial c_\pm}{\partial y} \pm \frac{Fq}{RT}c_\pm \frac{\partial \phi}{\partial y}\right) = \begin{cases} \frac{\partial \Gamma}{\partial t} \\ 0 \end{cases} \quad \text{on } y = 0, \tag{4.51}$$

$$\frac{\partial \phi}{\partial y} = \frac{4\pi F q}{\epsilon_p} S_T \Gamma \quad \text{on } y = 0. \tag{4.52}$$

Again the next step of our analysis is to non-dimensionalise our system of equations and their initial and boundary conditions. We introduce an arbitrary length scale L and we rescale our variables in the same manner as for the nonionic case. Obviously, we reintroduce the scaling RT/Fq for the electrical potential ϕ. On choosing L and τ to be the same values as in Section 4.1 ($L = L_{Diff} \approx 7.6 \times 10^{-6}$ m and $\tau \approx 0.12$ s), we find that

$$\omega_1 = \omega_2 \equiv \omega_{Diff} \approx 7.3 \times 10^{-4}, \tag{4.53}$$

where ω_1 and ω_2 are defined by (3.14) and (3.15). On dropping the stars, this gives the following non-dimensional set of equations, and initial and boundary conditions

$$\frac{\partial c_\pm}{\partial t} = \frac{\partial^2 c_\pm}{\partial y^2} \pm \frac{\partial}{\partial y}\left(c_\pm \frac{\partial \phi}{\partial y}\right), \tag{4.54}$$

$$\omega_{Diff}^2 \frac{\partial^2 \phi}{\partial y^2} = -(c_+ - c_-), \tag{4.55}$$

$$\frac{\partial \Gamma}{\partial t} = T\left[c_{+s}(1 - \Gamma) - \beta e^{-\phi_0}\Gamma\right], \tag{4.56}$$

$$c_\pm(y,0) = 1, \quad \Gamma(0) = 0, \tag{4.57}$$

$$\phi \to 0 \quad \text{as } y \to -\infty, \tag{4.58}$$

$$c_\pm \to 1 \quad \text{as } y \to -\infty, \tag{4.59}$$

$$-\left(\frac{\partial c_\pm}{\partial y} \pm c_\pm \frac{\partial \phi}{\partial y}\right) = \begin{cases} \frac{\partial \Gamma}{\partial t} \\ 0 \quad \text{on } y = 0, \end{cases} \tag{4.60}$$

$$\omega_{Diff}^2 \frac{\partial \phi}{\partial y} = S_T \Gamma \quad \text{on } y = 0. \tag{4.61}$$

4.2.1 Matched asymptotics

Since ω_{Diff}^2 is a small parameter and it multiplies the highest derivative in (4.55), we anticipate that there may be a boundary layer close to the free surface in which electrical effects become important. Note that from (3.17), $L_{Diff} \approx 7.6 \times 10^{-6}\,\mathrm{m}$, while $L_{Elec} \approx 5.6 \times 10^{-9}\,\mathrm{m}$.

Outer asymptotic solution

Far from the free surface, the terms multiplied by ω_{Diff}^2 in our equations are negligible so that, to leading order we have

$$\frac{\partial c_\pm}{\partial t} = \frac{\partial^2 c_\pm}{\partial y^2} \pm \frac{\partial}{\partial y}\left(c_\pm \frac{\partial \phi}{\partial y}\right), \tag{4.62}$$

$$c_+ - c_- = 0, \tag{4.63}$$

$$\frac{\partial \Gamma}{\partial t} = T\left[c_{+s}(1-\Gamma) - \beta e^{-\phi_0}\Gamma\right], \tag{4.64}$$

$$c_\pm(y,0) = 1, \quad \Gamma(0) = 0, \tag{4.65}$$

$$\phi \to 0 \quad \text{as } y \to -\infty, \tag{4.66}$$

$$c_\pm \to 1 \quad \text{as } y \to -\infty, \tag{4.67}$$

$$-\left(\frac{\partial c_\pm}{\partial y} \pm c_\pm \frac{\partial \phi}{\partial y}\right) = \begin{cases} \frac{\partial \Gamma}{\partial t} \\ 0 \quad \text{on } y = 0. \end{cases} \tag{4.68}$$

Now (4.63) tells us that $c_+ = c_- \equiv c$; and substituting this into (4.62) we get

$$\frac{\partial c}{\partial t} = \frac{\partial^2 c}{\partial y^2} \pm \frac{\partial}{\partial y}\left(c \frac{\partial \phi}{\partial y}\right), \tag{4.69}$$

which reduces to

$$\frac{\partial c}{\partial t} = \frac{\partial^2 c}{\partial y^2}, \tag{4.70}$$

i.e. the standard diffusion equation that we used to describe the nonionic case in Section 4.1. We cannot, however, satisfy both the conditions for $c_\pm$ in (4.68) which implies that we must indeed have a boundary layer. Our equation for ϕ has become

$$\frac{\partial}{\partial y}\left(c\frac{\partial \phi}{\partial y}\right) = 0, \tag{4.71}$$

and by using (4.66), we have $\phi \equiv 0$ in the outer solution. We impose the matching condition $c = c_{IN}$ on $y = 0$. Then in the outer region we are considering a problem identical to that for the time-dependent nonionic case studied in Section 4.1, but with a different boundary value on $y = 0$. Thus our solution in this region is

$$c(y,t) = 1 + \frac{1}{2\sqrt{\pi}}\int_0^t \frac{1 - c_{IN}(\tau)}{(t-\tau)^{3/2}}\, y \, \exp\frac{-y^2}{4(t-\tau)}\, d\tau. \tag{4.72}$$

Then, as with the system in Section 4.1, our outer region is governed by the equations

$$\frac{d\Gamma}{dt} = T\left[c_{+s}(1-\Gamma) - \hat{\beta}\Gamma\right] = \frac{1}{\sqrt{\pi}}\frac{d}{dt}\int_0^t \frac{(1 - c_{IN})}{\sqrt{t-\tau}}\, d\tau. \tag{4.73}$$

Inner asymptotic solution

Since, as noted earlier, we cannot satisfy (4.68) we have a boundary layer close to the free surface in which the c_+ and c_- must differ. We rescale y by writing $y = \omega_{Diff}\zeta$, so that now we have

$$\omega_{Diff}^2 \frac{\partial c_\pm}{\partial t} = \frac{\partial^2 c_\pm}{\partial \zeta^2} \pm \frac{\partial}{\partial \zeta}\left(c_\pm \frac{\partial \phi}{\partial \zeta}\right), \tag{4.74}$$

$$\frac{\partial^2 \phi}{\partial \zeta^2} = -(c_+ - c_-), \tag{4.75}$$

$$c_\pm(\zeta, 0) = 1, \quad \Gamma(0) = 0, \tag{4.76}$$

$$-\left(\frac{\partial c_\pm}{\partial \zeta} \pm c_\pm \frac{\partial \phi}{\partial \zeta}\right) = \begin{cases} \omega_{Diff}\frac{\partial \Gamma}{\partial t} \\ 0 \quad \text{on } \zeta = 0, \end{cases} \tag{4.77}$$

$$\omega_{Diff}\frac{\partial \phi}{\partial \zeta} = S_T \Gamma \quad \text{on } \zeta = 0, \tag{4.78}$$

and the conditions $\phi \to 0$, $c_\pm \to c_{IN}$ as $\zeta \to -\infty$ to match up with the outer region. Note that the evolution equation for Γ (4.64) remains unchanged by this change of variables. c_{+s} is, however, evaluated just below the free surface and is thus at the top of the electrical boundary layer.

Now we write our functions $c_\pm$, ϕ, Γ as series expansions in ω_{Diff}^2, of the form

$$c_\pm(\zeta,t) \approx c_\pm^{(0)}(\zeta,t) + \omega_{Diff}^2 c_\pm^{(1)}(\zeta,t) + \omega_{DIff}^4 c_\pm^{(2)}(\zeta,t) + ..., \tag{4.79}$$

$$\phi(\zeta,t) \approx \phi^{(0)}(\zeta,t) + \omega_{Diff}^2 \phi^{(1)}(\zeta,t) + \omega_{Diff}^4 \phi^{(2)}(\zeta,t) + ..., \tag{4.80}$$

$$\Gamma(t) \approx \Gamma^{(0)}(t) + \omega_{Diff}^2 \Gamma^{(1)}(t) + \omega_{Diff}^4 \Gamma^{(2)}(t) + ... \tag{4.81}$$

Substituting these expansions into (4.74) to (4.78) and taking $\omega_{Diff}/S_T = O(1)$, to lowest order we get (dropping superscripts)

$$\frac{\partial^2 c_\pm}{\partial \zeta^2} \pm \frac{\partial}{\partial \zeta}\left(c_\pm \frac{\partial \phi}{\partial \zeta}\right) = 0, \tag{4.82}$$

$$\frac{\partial^2 \phi}{\partial \zeta^2} = -(c_+ - c_-), \tag{4.83}$$

$$\phi = \phi_0 \quad \text{on } \zeta = 0, \tag{4.84}$$

$$c_\pm = c_{\pm s} \quad \text{on } \zeta = 0, \tag{4.85}$$

$$-\left(\frac{\partial c_\pm}{\partial \zeta} \pm c_\pm \frac{\partial \phi}{\partial \zeta}\right) = 0 \quad \text{on } \zeta = 0, \tag{4.86}$$

$$\frac{\partial \phi}{\partial \zeta} = S_T^* \Gamma \quad \text{on } \zeta = 0, \tag{4.87}$$

where $S_T^* = S_T/\omega_{Diff}$. We still have the matching condition

$$\phi \to 0,\ c_\pm \to c_{IN} \text{ as } \zeta \to -\infty. \tag{4.88}$$

Now, integrating (4.82) twice and applying conditions (4.84), (4.85), (4.86), and (4.88), we acquire

$$c_\pm = c_{IN} \exp(\mp\phi), \tag{4.89}$$

$$c_{IN} = c_{+s} \exp(\phi_0), \tag{4.90}$$

so that in the inner region our system is governed by (4.87), (4.90) and

$$\frac{\partial^2 \phi}{\partial \zeta^2} = 2 c_{IN} \sinh \phi. \tag{4.91}$$

Now, integrating (4.91) and applying the condition (4.88) we obtain an expression for ϕ_ζ in terms of c_{IN} and $\sinh(\phi_0/2)$ on $\zeta = 0$. Substituting in our expression (4.90) and equating this with (4.87), we completely eliminate ϕ from our calculations, to leave us with

$$S_T^* \Gamma = \sqrt{2}\, \frac{c_{IN} - c_{+s}}{\sqrt{c_{+s}}}. \tag{4.92}$$

4.2.2 The Abel equations and the numerical scheme

Bringing (4.73) and (4.92) together, writing $c_{IN}(t) = 1 - \psi_{IN}(t)$, $c_{+s}(t) = 1 - \psi_{+s}(t)$, and inverting these as before in Section 4.1, we obtain a set of three simultaneous Abel equations

$$\Gamma(t) = \frac{1}{\sqrt{\pi}} \int_0^t \frac{\psi_{IN}(\tau)}{\sqrt{t-\tau}}\, d\tau, \tag{4.93}$$

$$\psi_{IN}(t) = \frac{T}{\sqrt{\pi}} \int_0^t \frac{[(1-\psi_{+s}(\tau))(1-\Gamma(\tau)) - \beta\Gamma(\tau)]}{\sqrt{t-\tau}}\, d\tau, \tag{4.94}$$

$$S_T^* \Gamma \sqrt{1-\psi_{+s}(t)} = \sqrt{2}\,(\psi_{+s}(t) - \psi_{IN}(t))\,. \tag{4.95}$$

We use a similar numerical scheme as the one found in Section 4.1, giving us two simultaneous nonlinear equations for ψ_{IN}^n, ψ_{+s}^n, and Γ^n of the form

$$\psi_{IN}^n = A + B\psi_{+s}^n + C\Gamma^n + D\psi_{+s}^n\Gamma^n, \tag{4.96}$$

$$\Gamma^n = a + b\psi_{IN}^n, \tag{4.97}$$

$$S_T^* \Gamma^n \sqrt{1-\psi_{+s}^n} = \sqrt{2}\,\left(\psi_{+s}^n - \psi_{IN}^n\right), \tag{4.98}$$

where a, b, A, B, C, D are as in the nonionic case except that in a we replace ψ_j by ψ_{IN}^j and in A and C we replace ψ_j by ψ_{+s}^j. We rewrite (4.96) to (4.98) as

$$F_1\left(\Gamma^n, \psi_{+s}^n, \psi_{IN}^n\right) = a + b\psi_{IN}^n - \Gamma^n = 0, \tag{4.99}$$

$$F_2\left(\Gamma^n, \psi_{+s}^n, \psi_{IN}^n\right) = A + B\psi_{+s}^n + C\Gamma^n + D\psi_{+s}^n\Gamma^n - \psi_{IN}^n = 0, \tag{4.100}$$

$$F_3\left(\Gamma^n, \psi_{+s}^n, \psi_{IN}^n\right) = S_T^*\Gamma^n\sqrt{1-\psi_{+s}^n} - \sqrt{2}\,\left(\psi_{+s}^n - \psi_{IN}^n\right) = 0, \tag{4.101}$$

i.e. $\mathbf{F}(\mathbf{x}) = \mathbf{0}$ where

$$\mathbf{x} = \begin{pmatrix} \Gamma^n \\ \psi_{+s}^n \\ \psi_{IN}^n \end{pmatrix}.$$

We let $\mathbf{F}'(\mathbf{x})$ be the Jacobian matrix, i.e. $(\mathbf{F}'(\mathbf{x}))_{\mathbf{ij}} = \partial \mathbf{F_i}/\partial \mathbf{x_j}$, given by

$$\mathbf{F}'(\mathbf{x}) = \begin{pmatrix} -1 & 0 & b \\ C + D\psi_{+s}^n & B + D\Gamma^n & -1 \\ S_T^*\sqrt{1-\psi_{+s}^n} & -1/2\, S_T^*\,\Gamma^n\left(1-\psi_{+s}^n\right)^{-1/2} - \sqrt{2} & \sqrt{2} \end{pmatrix}.$$

To find $\mathbf{x}$ we use Newton's method. We solve this set of equations using Fortran and we view how Γ and $c_{\pm s}$ behave with time for different values of S_T in Figures 4.8 to 4.11. We note that, for each value of S_T chosen, $\hat{\beta}$ will correspondingly change according to the relation (3.25) for the steady-state problem

$$\hat{\beta} = \beta e^{-\phi_{0ss}},$$

where ϕ_{0ss} is the value of ϕ_0 associated with S_T obtained from the steady-state problem. We use the values of S_T and $\hat{\beta}$ given at the end of Chapter 3, and we show solutions for these values in Figures 4.8 to 4.11. The Fortran coding for this scheme may be found in Appendix C.

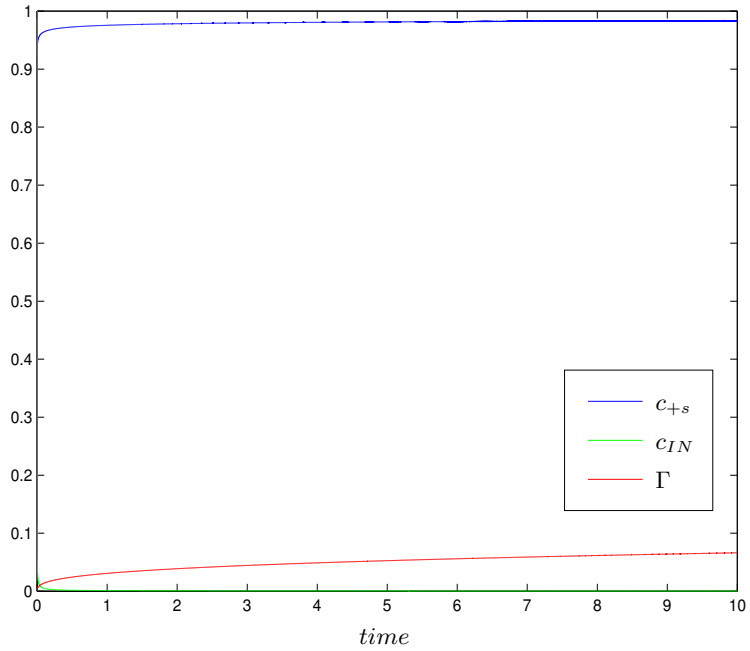


Figure 4.8: Surface concentration Γ, subsurface concentration c_{+s}, and the matching concentration c_{IN} against time ($S_T = 1$, $\hat{\beta} \approx 2.3 \times 10^{-7}$, $T = 10$).

4.2.3 Discussion of results

Examining Figures 4.10 and 4.11 we see that, as with the nonionic case, both Γ and c_{+s} tend towards their steady-state values of $1/(\hat{\beta}+1)$ and 1 respectively as $t \to \infty$, for each value of $\hat{\beta}$; showing that over large time scales the nonionic and ionic systems behave alike. Indeed, c_{+s} returns to its steady-state value very slowly. As we saw in Chapter 3, a decrease in the value of the Stern constant S_T from 1 through ω_{Diff} to ω_{Diff}^2 corresponds to an increase in the number of bound cations on the surface and hence a decrease in the size of the surface electrical potential ϕ_0.

For $S_T = 1$, we have a large value of the surface potential which will slow down the rate at which the cations adsorb onto the surface. A low rate of adsorption onto the surface means that very few of the subsurface cations are transported to the surface. Meanwhile, this tiny depletion in the subsurface concentration c_{+s} means that the diffusion of these ions from the bulk solution to the subsurface is nearly nonexistent.

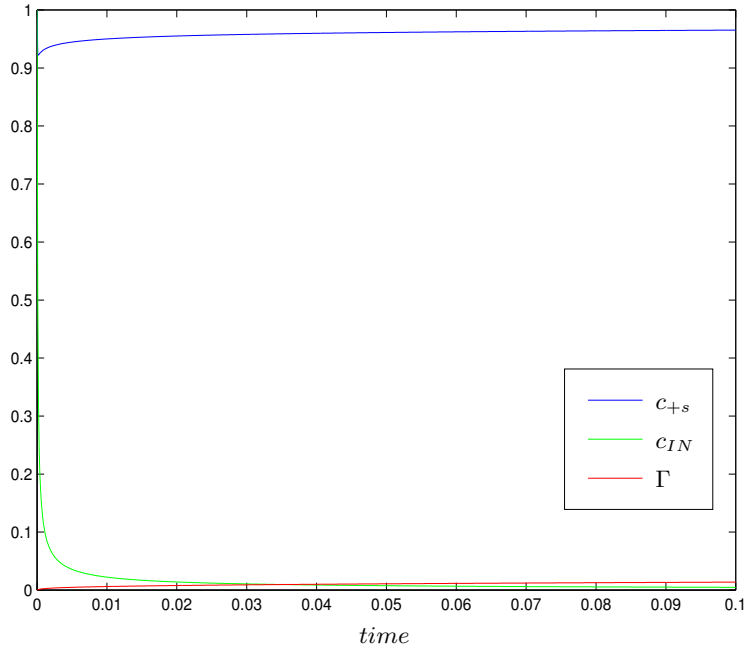


Figure 4.9: Surface concentration Γ, subsurface concentration c_{+s}, and the matching concentration c_{IN} against time (close up) ($S_T = 1$, $\hat{\beta} \approx 2.3 \times 10^{-7}$, $T = 10$).

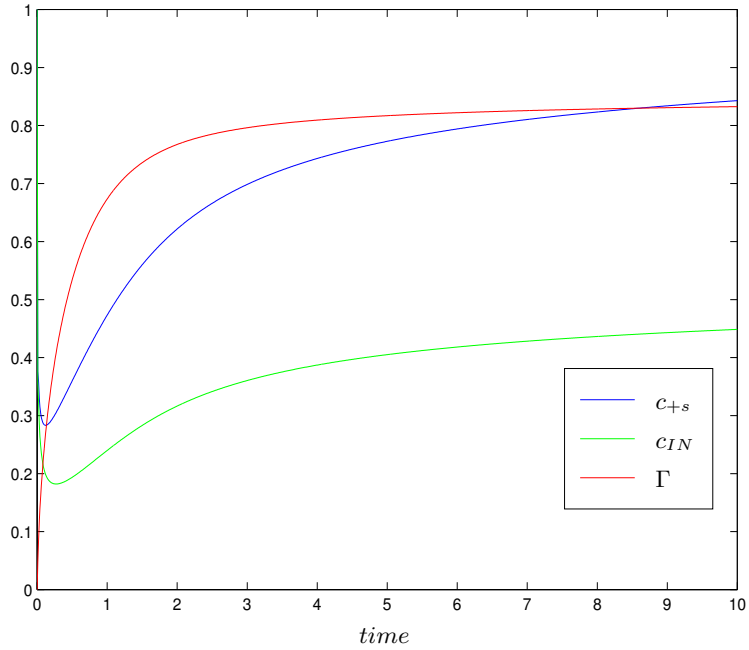


Figure 4.10: Surface concentration Γ, subsurface concentration c_{+s}, and the matching concentration c_{IN} against time ($S_T = \omega$, $\hat{\beta} \approx 0.09$, $T = 10$).

This is what is happening in Figure 4.8 and 4.9. Here, both c_{IN} and c_{+s} initially decrease: c_{IN} tending straight to zero as the diffusion from the bulk solution is negligible, and c_{+s} only decreasing slightly as surface adsorption is negligible. Hence, only a tiny increase in surface concentration Γ on this graph is seen.

Now, for smaller surface potentials (corresponding to our decreasing values of S_T) the rate at which the cations are adsorbed onto the surface is increased because there is less of a repulsive force. Hence more subsurface cations are transported to the surface. Again, this depletion in the subsurface causes the diffusion process to act, carrying cations from the bulk solution to the subsurface. This is what is happening in Figures 4.10 and 4.11. Again, both c_{IN} and c_{+s} initially decrease while Γ increases as the cations are adsorbed onto the surface. c_{IN} and c_{+s} then increase as diffusion takes effect. c_{IN} and c_{+s} are essentially identical for $S_T = \omega_{Diff}^2$ (in Figure 4.11) because the surface potential ϕ_0 is essentially zero and we are, in effect, looking at a situation in which ionic effects are negligible. This can be seen by directly comparing Figure 4.11 with Figure 4.1 at the beginning of this chapter.

The idea of this asymptotic approach was to split the fluid adjacent to the adsorbed layer into two regions of different thickness (refer back to Figure 1.2). The inner region is the electrical double layer where the electric potential ϕ decays from its surface value ϕ_0 to zero in the bulk solution. This layer is of characteristic length $L_{Elec} \approx 5.6 \times 10^{-9}\,\mathrm{m}$. The outer region is the diffusion layer created by concentration gradients provoked by the disturbance of the adsorption layer. This region is of a characteristic length $L_{Diff} \approx 7.6 \times 10^{-6}\,\mathrm{m}$.

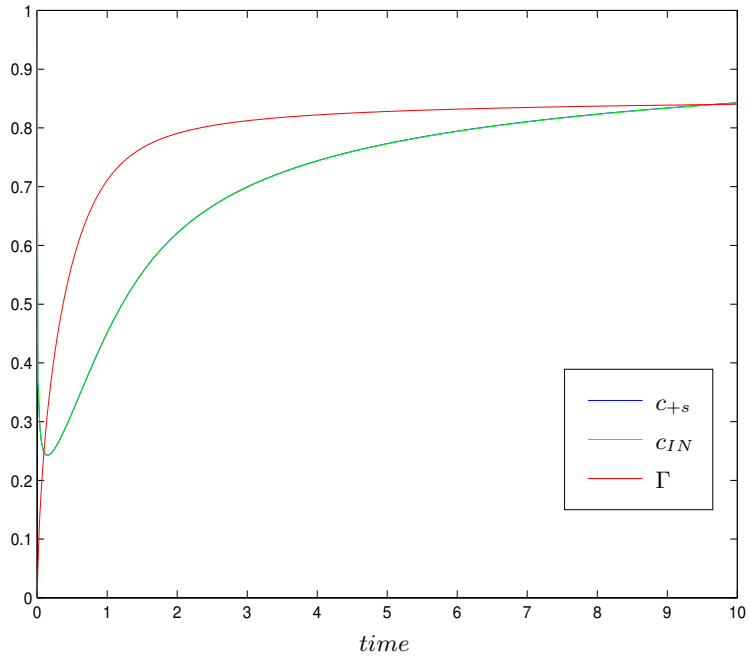


Figure 4.11: Surface concentration Γ, subsurface concentration c_{+s}, and the matching concentration c_{IN} against time ($S_T = \omega^2$, $\hat{\beta} \approx 0.16$, $T = 10$). Note that c_{+s} is not visible since it is approximately 10^{-7} away from c_{IN}.

Chapter 5

The non-static, steady-state nonionic problem

We go on now to look at the problem of the non-static, steady-state nonionic surfactant system. As mentioned in the introduction, this problem was tacked in Breward *et al.* [7], yet they were unable to fix one parameter in their solution. Here we present a method for determining this parameter and go on to show that it gives a well behaved solution to the subsurface concentration c_s near the edge of the cylinder.

With the reintroduce of motion into our problem, we may no longer assume that all the surfactant dynamics take place solely in the y-direction. Our velocity $\mathbf{u}$ is then governed by the steady-state versions of (2.1), (2.2), and boundary conditions (2.3) to (2.6).

Without initially presenting our governing equations and their boundary conditions, we go straight onto non-dimensionalising our system by introducing an arbitrary length scale L and a dilatation rate α, and scaling our variables as follows

$$\begin{aligned} \mathbf{x} &= L\mathbf{x}^*, \\ c_\pm &= c_b c_\pm^*, \\ \Gamma &= \Gamma_{sat}\Gamma^*, \\ \gamma &= \gamma_w \gamma^*, \\ \mathbf{u} &= \alpha L \mathbf{u}^*, \\ p &= \rho\alpha^2 L^2 p^*. \end{aligned}$$

Now, we define the Marangoni number by $M_a = Re^{-1/2}\Delta\gamma/\mu\alpha L$, where $\Delta\gamma$ is the magnitude of the surface tension change which can be related to changes in Γ and c_s

by

$$\Delta\Gamma \sim \frac{L^2(\rho\mu\alpha^3)^{1/2}}{RT}, \tag{5.1}$$

$$\frac{\Delta c_s}{c_b} \sim \frac{L^2(\rho\mu\alpha^3)^{1/2}}{\Gamma_{sat}RT}. \tag{5.2}$$

And we define $\Lambda = RT\Gamma_{sat}/\gamma_w$. We pick L, α, ϵ_h and ϵ_d such that $Re\epsilon_h$, $Pe\epsilon_d$, and $Ma\Lambda$ are equal to 1.

By the argument presented in Howell and Breward [12], we have a high Reynold's number flow, Re, (of the order of 10^2). The dimensionless hydrodynamic equation for our system is

$$\mathbf{u}\cdot\nabla\mathbf{u} = -\nabla p + \frac{1}{Re}\nabla^2\mathbf{u}. \tag{5.3}$$

Meanwhile, the dimensionless advection-diffusion equation for our surfactant dynamics is

$$\mathbf{u}\cdot\nabla c = \frac{1}{Pe}\nabla^2 c, \tag{5.4}$$

where the Péclet number Pe is of the order 10^5. We may treat the fluid flow as inviscid outside a viscous boundary layer at the free surface. Inside this hydrodynamic boundary layer of thickness $LRe^{-1/2}$, the x-momentum and incompressibilty equations for the Navier-Stokes equations, after much simplification, become

$$u\frac{\partial u}{\partial x} + v_h\frac{\partial u}{\partial y_h} = \frac{\partial^2 u}{\partial y_h^2}, \tag{5.5}$$

$$\frac{\partial u}{\partial x} + \frac{\partial v_h}{\partial y_h} = 0, \tag{5.6}$$

where y_h and v_h are the boundary layer variables (i.e $y = \epsilon_h y_h$, $v = \epsilon_h v_h$, where $\epsilon_h = Re^{-1/2}$. Advection dominates the surfactant system and so c is effectively equal to the bulk concentration, 1, to lowest order far from the surface. However, this "outer solution" violates the free surface boundary conditions, and thus a diffusive boundary layer must be introduced near $y = 0$. Inside this boundary layer (thickness $LPe^{-1/2}$) we may neglect diffusion in the x-direction so that c now satisfies

$$u\frac{\partial c}{\partial x} + v_d\frac{\partial c}{\partial y_d} = \frac{\partial^2 c}{\partial y_d^2}, \tag{5.7}$$

where y_d and v_d are the boundary layer variables (i.e. $y = \epsilon_d y_d$, $v = \epsilon_d v_d$, where $\epsilon_d = Pe^{-1/2}$.

The diffusive boundary layer is much thinner than the hydrodynamic boundary layer, so that across the diffusive boundary layer the radial velocity u is effectively uniform

and takes its value on the free surface. We may thus replace u by U_s (where $U_s(x) = u(x,0)$) in all equations governing the advection-diffusion dynamics of the surfactant.

For ease of notation we henceforth drop the "h" and "d" subscripts. (5.5) and (5.6) may then be rewritten along with the boundary and matching conditions for the boundary layer as

$$u\frac{\partial u}{\partial x} + v\frac{\partial u}{\partial y} = \frac{\partial^2 u}{\partial y^2}, \tag{5.8}$$

$$\frac{\partial u}{\partial x} + \frac{\partial v}{\partial y} = 0, \tag{5.9}$$

$$v = 0 \text{ on } y = 0, \tag{5.10}$$

$$u \to 0 \text{ as } y \to -\infty, \tag{5.11}$$

$$u = 0 \text{ on } x = 0, \tag{5.12}$$

and with $u = U_s$ on $y = 0$. The boundary condition representing the conservation of tangential momentum at the surface is now

$$\frac{\partial u}{\partial y} = M_a \frac{d\gamma}{dx} \quad \text{on } y = 0. \tag{5.13}$$

Dropping subscripts and using $v_d = -yU_{sx}$ in the diffusive boundary layer close to the surface, (5.7) may be rewritten as

$$U_s\frac{\partial c}{\partial x} - \frac{\partial U_s}{\partial x}y\frac{\partial c}{\partial y} = \frac{\partial^2 c}{\partial y}, \tag{5.14}$$

and the dimensionless steady-state version of the boundary condition representing conservation of surfactant at the interface (2.14) is

$$\frac{\partial c}{\partial y} = -\frac{d}{dx}\left(\frac{U_s c_s}{\beta + c_s}\right) \text{ on } y = 0. \tag{5.15}$$

The dimensionless version of the Frumkin equation (2.17) may be written as

$$\gamma - 1 = \Lambda \log(1 - \Gamma). \tag{5.16}$$

(5.16) may be differentiated with repsect to x to give

$$\frac{d\gamma}{dx} = -\Lambda\frac{1}{1-\Gamma}\frac{d\Gamma}{dx}, \tag{5.17}$$

where Γ_x may also be found by differentiating the dimensionless version of the Langmuir isotherm (3.5)

$$\frac{d\Gamma}{dx} = \frac{\beta}{(\beta + c_s)^2}\frac{dc_s}{dx} \text{ on } y = 0. \tag{5.18}$$

Eliminating Γ and Γ_x from (5.17) using (3.5) and (5.18) we are left with an equation relating the gradient in γ to the gradient in c_s on the surface

$$\frac{\partial \gamma}{\partial x} = -\frac{\Lambda}{\beta + c_s}\frac{dc_s}{dx} \text{ on } y = 0, \tag{5.19}$$

Substituting (5.19) into (5.13), the boundary condition representing the conservation of tangential momentum at the surface is now

$$\frac{\partial u}{\partial y} = -\frac{1}{\beta + c_s}\frac{dc_s}{dx} \text{ on } y = 0, \tag{5.20}$$

where we have used the fact that we have chosen α such that $Ma\Lambda = 1$. c is then governed by (5.14) with boundary conditions (5.15), (5.20) and

$$c \rightarrow 1 \text{ as } y \rightarrow -\infty, \tag{5.21}$$

$$\frac{\partial c}{\partial x} = 0 \text{ on } x = 0, \tag{5.22}$$

and we denote the subsurface concentration as $c = c_s(x)$ on $y = 0$. Note that in the system outlined above there are no specified boundary conditions at the edge of the cylinder $x = x_0$ (where $x_0 \approx 2$). The experimental results are thought to be independent of both the radius of the overflowing-cylinder and the details of the flow over the edge. Hence, we suspect that the behaviour near the origin should be locally determined. In a method similar to that outlined in Howell and Breward [12], we seek the solution as a coordinate expansion of the form

$$u(x, y) = x f_0'(y) + ..., \tag{5.23}$$

$$v(x, y) = -f_0(y) + ..., \tag{5.24}$$

$$c(x, y) = c_0(y) + ... \tag{5.25}$$

Then at lowest order in x, (5.8) to (5.12), and (5.14), (5.15) and (5.20) to (5.22) may be rearranged to give the problem

$$f_0''' + f_0 f_0'' - (f_0')^2 = 0, \tag{5.26}$$

$$f_0'(0) = \frac{1}{\pi}\left(\frac{(\beta + c_0(0))(1 - c_0(0))}{c_0(0)}\right)^2, \tag{5.27}$$

$$f_0(0) = 0, \tag{5.28}$$

$$f_0'(-\infty) = 0, \tag{5.29}$$

$$c_0(y) = 1 + (c_0(0) - 1)\text{erfc}\left(y\sqrt{f_0'(0)}\right). \tag{5.30}$$

$$\tag{5.31}$$

Now, for any given value of $c_0(0)$ we have a well-posed problem for $f_0(y)$ which can readily be solved numerically. However, c_0, corresponding to the subsurface concentration evaluated at the origin, is a parameter which must be specified, and cannot be predicted by the model. This was the difficulty encountered in Breward *et al.* [7]; and it is this that is precisely tackled in Howell and Breward [12] by selecting a particular value of $c_0(0)$, solving the system (5.27) to (5.31) which then gives us values of u, v, c near the centre of the cylinder $x = 0$. The equations for u, v, c in the boundary layer near the surface can then be solved and c_s plotted. We require a unique value of our shooting parameter $c_0(0)$ such as to keep c_s finite as $x \to x_0$. If our chosen value of $c_0(0)$ does not satisfy this requirement, we must go back and select a different value.

5.1 Numerical scheme

We solve the system (5.8) to (5.12), and (5.14), (5.15) and (5.20)to (5.22) by applying an implicit central difference scheme. We firstly replace y with $-y$ in the equations (4.7) to (4.12) since we must discretise a positive interval for our scheme. A first-order difference is used to march in the x-direction, such that the problem to be solved at each new value of x is linear. We divide $(0, x)$ into N uniform intervals of width Δx so that $x_n = n\Delta x$. We truncate at a final depth L_d in the y-direction and discretise the interval $[0, L_d]$ using a uniform mesh: $y_j = j\Delta y$, $\Delta y = L_d/J$ for some integer J. We then have the finite difference scheme: for $j = 1, 2, ..., J-1$ and $n = 1, 2, ..., N-1$

$$\frac{1}{2}\left(\frac{u_j^n - u_j^{n-1}}{\Delta x} + \frac{u_{j-1}^n - u_{j-1}^{n-1}}{\Delta x}\right) + \frac{v_j^n - v_{j-1}^n}{\Delta y} = 0, \tag{5.32}$$

$$u_j^{n-1}\left(\frac{u_j^n - u_j^{n-1}}{\Delta x}\right) + v_j^n\left(\frac{u_{j+1}^{n-1} - u_{j-1}^{n-1}}{2\Delta y}\right) = \left(\frac{u_{j+1}^n - 2u_j^n + u_{j-1}^n}{(\Delta y)^2}\right), \tag{5.33}$$

$$u_0^{n-1}\left(\frac{c_j^n - c_j^{n-1}}{\Delta x}\right) + j\Delta y\left(\frac{u_0^n - u_0^{n-1}}{\Delta x}\right)\left(\frac{c_{j+1}^{n-1} - c_{j-1}^{n-1}}{2\Delta y}\right) = \left(\frac{c_{j+1}^n - 2c_j^n + c_{j-1}^n}{(\Delta y)^2}\right), \tag{5.34}$$

with the boundary conditions

$$\left(\frac{u_1^n - u_{-1}^n}{2\Delta y}\right) = \left(\frac{c_0^n - c_0^{n-1}}{\Delta x}\right)\left(\frac{1}{\beta + c_0^{n-1}}\right), \tag{5.35}$$

$$\left(\frac{c_1^n - c_{-1}^n}{2\Delta y}\right) = \left(\frac{u_0^{n-1}}{\beta + c_0^{n-1}}\right)\left(\frac{c_0^n - c_0^{n-1}}{\Delta x}\right) + \left(\frac{c_0^{n-1}}{\beta + c_0^{n-1}}\right)\left(\frac{u_0^n - u_0^{n-1}}{\Delta x}\right) \tag{5.36}$$

$$- \left(\frac{u_0^{n-1} c_0^{n-1}}{(\beta + c_0^{n-1})^2}\right)\left(\frac{c_0^n - c_0^{n-1}}{\Delta x}\right), \tag{5.37}$$

and $v_0^n = 0$, $u_J^n = 1$, $c_J^n = 1$.

To get the solution started, we have to choose a particular value of $c_0(0)$; then the known local behaviour (5.24) to (5.25) is used to initialise u and c at a small but finite value of x.

We solve this system using Matlab and we show how c and u behave in the hydrodynamic boundary layer in Figures 5.1 to 5.6. The Matlab coding for this scheme may be found in Appendix D.

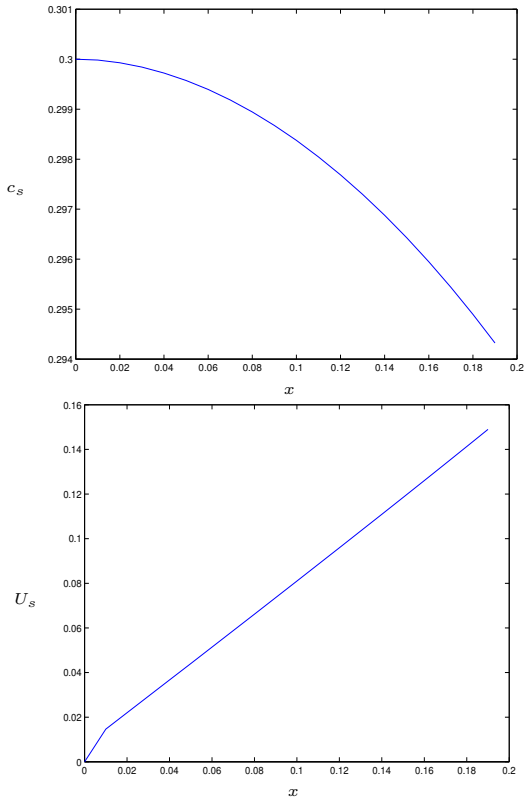


Figure 5.1: Surface velocity U_s and subsurface concentration c_s versus coordinate x, for the parameter values $c_b = 0.5\,\text{mol m}^{-3}$, $a = 0.04\,\text{m}$, $c_s(0) = 0.3$.

5.1.1 Discussion of results

We start with a relatively low value of 0.3 for the value of $c_s(0)$ and plot the resulting variations of U_s and c_s with x in Figure 5.1. We can see that, near the origin, U_s is approximately linear. The corresponding plots of u and c versus depth are shown in Figure 5.2 at various values of x. We see that for increasing x, the variations in u and c are confined to increasingly narrow boundary layers near $y = 0$. Figures

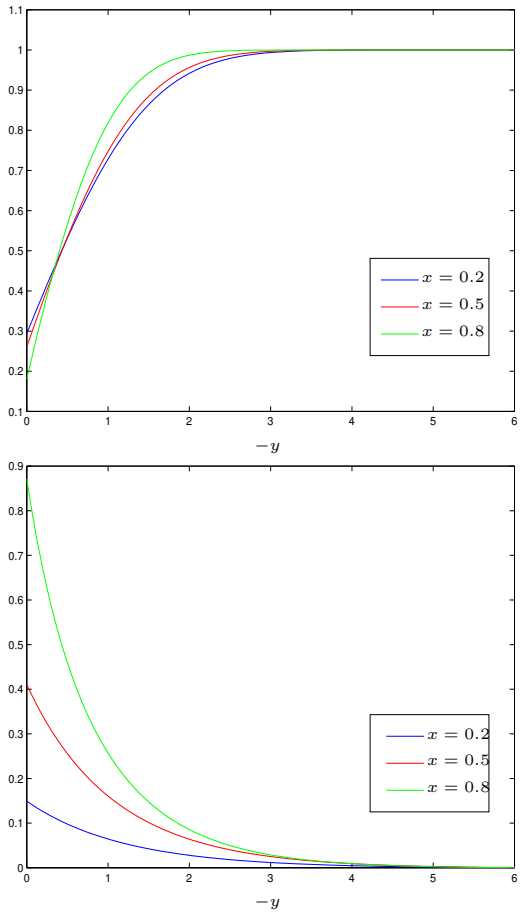


Figure 5.2: Radial velocity u and concentration c versus depth y, for the same parameter values as in Figure 5.1.

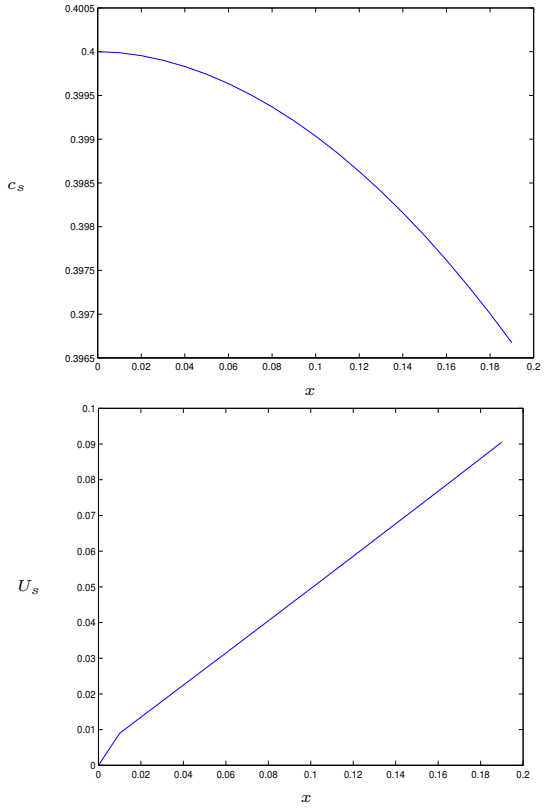


Figure 5.3: Surface velocity U_s and subsurface concentration c_s versus coordinate x, for the parameter values $c_b = 0.5\,\mathrm{mol\ m^{-3}}$, $a = 0.04\,\mathrm{m}$, $c_s(0) = 0.4$.

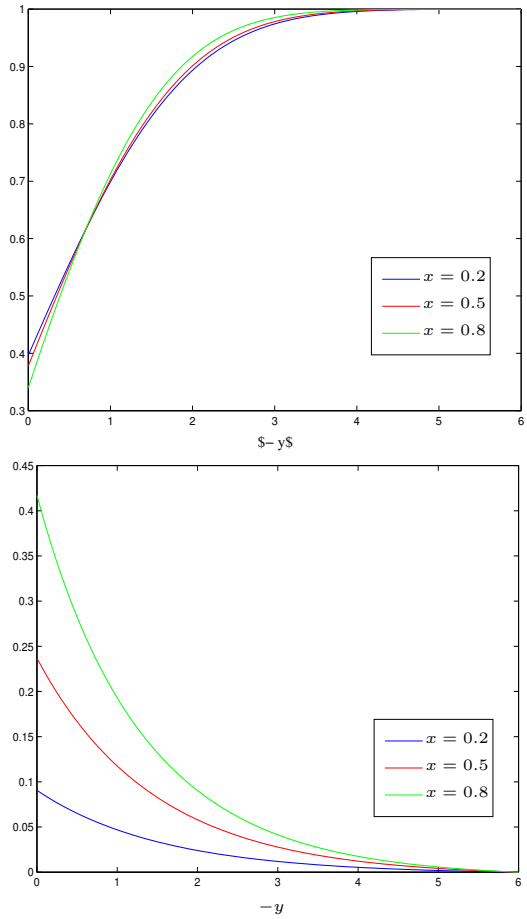


Figure 5.4: Radial velocity u and concentration c versus depth y, for the same parameter values as in Figure 5.3.

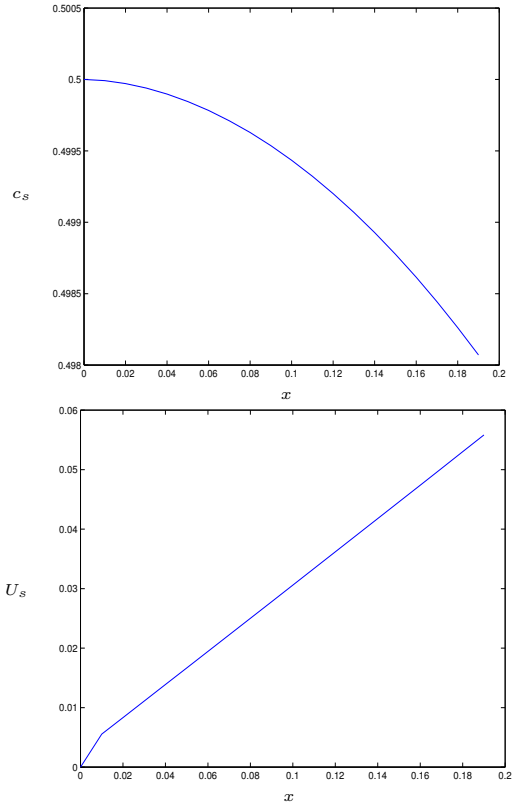


Figure 5.5: Surface velocity U_s and subsurface concentration c_s versus coordinate x, for the parameter values $c_b = 0.5\,\mathrm{mol\ m^{-3}}$, $a = 0.04\,\mathrm{m}$, $c_s(0) = 0.5$.

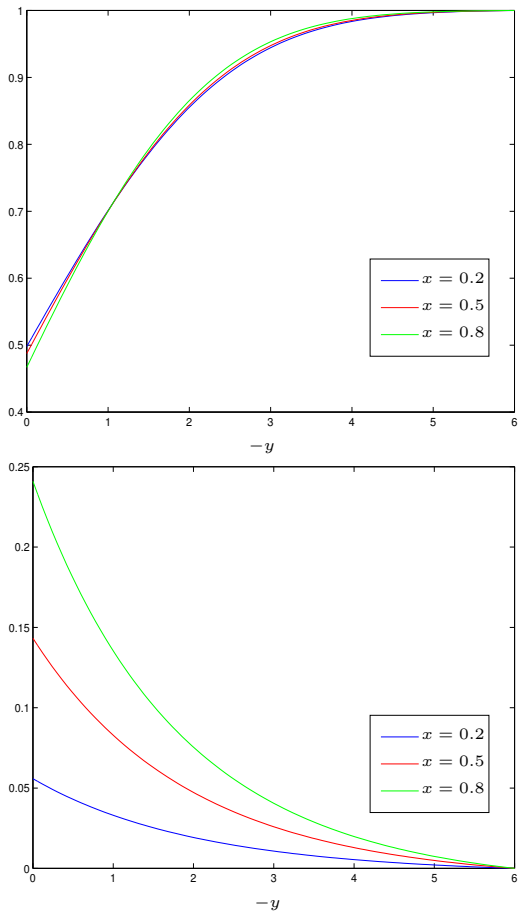


Figure 5.6: Radial velocity u and concentration c versus depth y, for the same parameter values as in Figure 5.5.

5.3 and 5.5 show the behaviour of U_s and c_s for the same parameter values but with larger values of $c_s(0) = 0.4$, 0.5 respectively. For both of these we see that U_s behaves approximately linearly near $x = 0$. Although it is not shown here, plotting for greater x shows that for $c_s(0) = 0.5$, c_s does not reach zero as x approaches $x_0 \approx 2$. In fact c_s blows up as $x \to x_0$ while U_s tends to zero. This can be seen from the results given in Howell and Breward [12]. The corresponding values of u and c are shown in Figure 5.4. The velocity at depth remains small. The concentration varies only slightly with x. As shown in Breward and Howell [12], a value of $c_s(0) = 0.4$ is close to the critical value we require to keep c_s finite as x tends to x_0. The variation of U_s and c_s with x are shown in Figure 5.3 for x only up to 0.2. In Figure 5.4 we see the variation of u and c with depth in the same parameter regime for values of x increasing.

Chapter 6

Conclusions & Discussion

As prescribed in the introductory section of this project, the aims of this study were firstly to obtain a model and investigate the behaviour of an ionic surfactant at an air-water interface, and secondly to generate a numerical simulation of the governing equations for a nonionic surfactant on a finite domain.

In Chapter 2, we presented the equations governing the fluid and surfactant dynamics of the over-flowing cylinder experiment. In Chapter 3, we looked at the static steady-state surfactant problem and presented a method for calculating the values of ϕ_0 for each chosen value of the Stern constant S_T. This then allowed us to calculate the value of $\hat{\beta}$ using relation (3.25) which, in turn, is used to calculate the value of the surface concentration Γ using the altered Langmuir isotherm (3.27). We then went on to Chapter 4 where we considered the static time-dependent surfactant problem, addressing both the nonionic and ionic cases separately. The latter case showed us that we could effectively split the fluid adjacent to the adsorbed layer into two regions of different thickness: the inner region being the electrical double layer where the electric potential ϕ decays from its surface value ϕ_0 to zero in the bulk solution; the outer region being the diffusion layer created by concentration gradients provoked by the disturbance of the adsorption layer. In Chapter 5, we looked at the problem of the nonstatic nonionic surfactant problem which is the subject of Breward *et al.* [7], and Howell and Breward [12]. It was possible (with the help of Howell and Breward [12]) to decipher the unknown parameter $c_s(0)$ by use of a shooting method, which then enabled us to produce the corresponding u and c profiles in the boundary layer near the surface.

A possible extension to this study is finding the parameter $c_s(0)$ to a higher degree of accuracy than was achieved here. Furthermore, the ionic model could be used for

looking at the nonstatic ionic surfactant problem which would help in the assessment of ionic effects on an expanding free surface. However, the results produced in this examination have implied that ionic effects are only small. Hence, further studies may show that these ionic effects, whilst present, are negligible when compared to the adsorption and advection-diffusion processes occuring in the fluid. Then ionic effects would not be the sole factor causing the discrepancies between theoretical and experimental evaluations of the dilitation rate. Other possible reasons for these discrepancies might be that the actual experiment had not been left for long enough to allow it to settle down to a state of equilibrium. Thus, a steady-state model for the experiment would be inaccurate and some time-dependency would have to be included.

Appendix A

Numerical scheme for the nonionic Abel equations

```
      program csabel
      implicit none
      integer n
      double precision delt,T,beta
      parameter (n=1000,delt=0.01d0,T=10.d0,beta=0.148d0)
      double precision tt(0:n),gamma(0:n),phi(0:n)
      double precision aa,bb,A,B,C,D,pi,dij
      integer i,j
c
      do i=0,n
         tt(i)=dble(i)*delt
      end do
c
      phi(0)=0.d0
      gamma(0)=0.d0
c
      pi=2.d0*asin(1.d0)
      bb=4.d0*dsqrt(delt/pi)/3.d0
      D=16.d0*T*dsqrt(delt/pi)/15.d0
c
      do i=1,n
         print*, i
         B=T*dsqrt(delt/pi)*(-20.d0+4.d0*gamma(i-1))/15.d0
```

```
      C=T*dsqrt(delt/pi)*(-20.d0*(1.d0+beta)+4.d0*phi(i-1))/15.d0
      aa=phi(i-1)
      A=30.d0-10.d0*(phi(i-1)+(1.d0+beta)*gamma(i-1))+6.d0*phi(i-1)
     &       *gamma(i-1)
      do j=0,i-2
         dij=dble(i-j)
         aa=aa+dsqrt(dij-1.d0)*(2.d0*(dij-1.d0)*phi(j)-(2.d0*dij+1.d0
     &          )*phi(j+1))+dsqrt(dij)*(2.d0*dij*phi(j+1)-(2.d0*dij-3
     &          .d0)*phi(j))
         A=A+dsqrt(dij-1.d0)*(-30.d0-20.d0*(dij-1.d0)*(phi(j)+(1.d0
     &          +beta)*gamma(j))+10.d0*(2.d0*dij+1.d0)*(phi(j+1)+(1.d0
     &          +beta)*gamma(j+1))-16.d0*(dij-1.d0)**2*phi(j)*gamma(j)
     &          -(16.d0*dij**2+8.d0*dij+6.d0)*phi(j+1)*gamma(j+1)+4
     &          .d0*(dij-1.d0)*(4.d0*dij+1.d0)*(phi(j)*gamma(j+1)+phi(j
     &          +1)*gamma(j)))
         A=A+dsqrt(dij)*(30.d0+10.d0*(2.d0*dij-3.d0)*(phi(j)+(1.d0
     &          +beta)*gamma(j))-20.d0*dij*(phi(j+1)+(1.d0+beta)
     &          *gamma(j+1))+(16.d0*dij**2-40.d0*dij+30.d0)*phi(j)
     &          *gamma(j)+16.d0*dij**2*phi(j+1)*gamma(j+1)-4.d0*dij*(4
     &          .d0*dij-5.d0)*(phi(j)*gamma(j+1)+phi(j+1)*gamma(j)))
      end do
      aa=aa*2.d0*dsqrt(delt/pi)/3.d0
      A=A*T*dsqrt(delt/pi)/15.d0
c
      if ((1.d0-aa*D-bb*C-B)**2-4.d0*bb*D*(A+aa*C) .lt. 0.d0) then
         print*, (1.d0-aa*D-bb*C-B)**2-4.d0*bb*D*(A+aa*C), 'err'
      else
      end if
c
      phi(i)=(1.d0-aa*D-bb*C-B-dsqrt((1.d0-aa*D-bb*C-B)**2-4.d0*bb*D
     &       *(A+aa*C)))/(2.d0*bb*D)
      gamma(i)=aa+bb*phi(i)
    end do
c
    open(14,file='abel.dat',status='unknown')
    write(14,50)(tt(i),1.d0-phi(i),gamma(i),i=0,n)
```

```
 50   format(3(f20.10))
c
      end
```

Appendix B

Numerical scheme for the diffusion equation

```
function p = diff(dt, tfinal, dz, zfinal, T, beta)
m = 1 + zfinal/dz;
n = 1 + tfinal/dt;
m1 = m + 1;
m2 = m + 2;
mu = dt/(dz^2);
nu = dz/dt;
c Initialization
for i = 1:m1,
        v(i) = 1;
        A = zeros(m2,m2);
        B = zeros(m2,m2);
end
v(m2) = 0;
p = v';
for i = 1:m1,
        c(i,1) = 1;
end
for t1 = 2:n,
         A(1,1) = -(mu+1);
         A(1,2) = mu;
         A(1,m2) = -mu*nu;
         for i = 2:m,
```

```
                A(i,i-1) = mu;
                A(i,i) = -(2*mu+1);
                A(i,i+1) = mu;
        end
        A(m1,m1) = 1;
        A(m2,1) = -dt*T*(1 - p(m2));
        A(m2,m2) = 1;

        B(1,1) = -1;
        B(1,m2) = -mu*nu;

        for i = 2:m,
                B(i,i) = -1;
        end
        B(m1,m1) = 1;
        B(m2,m2) = 1 - dt*T*beta;

c Ap^(n+1) = Bp^n

        C = A \ B;
        p = C*p;
        for i = 1:m1,
                c(i,t1) = p(i);
        end
        Gamma(t1) = p(m2);
end

figure
t=(0:n-1)*dt;
z=(0:m)*dz;
surf(t,z,c)
figure
plot(t,Gamma,'r')
hold on
plot(t,c(1,:))
```

Appendix C

Numerical scheme for the ionic Abel equations

```
c
      program csabel
      implicit none
      integer n
      double precision delt,T,beta,w,sT
      parameter (n=100000,delt=0.0001d0,T=10.d0,beta=2.3e-7,w=7.3e-4
     &     ,sT=1)
      double precision tt(0:n),gamma(0:n),phi_in(0:n),phi_s(0:n),s(3)
     &     ,x(3),f(3),fp(3,3),works(3)
      double precision aa,bb,A,B,C,D,pi,dij,tol,sw
      integer i,j,ia,ifail
      logical loop
      external F04ARF
c
c set up nonlinear tolerance
c
      tol=1.e-10
      ia=3
      sw=sT/w
c
      do i=0,n
         tt(i)=dble(i)*delt
      end do
```

```
c
      phi_in(0)=0.d0
      phi_s(0)=0.d0
      gamma(0)=0.d0
c
      pi=2.d0*asin(1.d0)
      bb=4.d0*dsqrt(delt/pi)/3.d0
      D=16.d0*T*dsqrt(delt/pi)/15.d0
c
      do i=1,n
         print*, i
         B=T*dsqrt(delt/pi)*(-20.d0+4.d0*gamma(i-1))/15.d0
         C=T*dsqrt(delt/pi)*(-20.d0*(1.d0+beta)+4.d0*phi_s(i-1))/15.d0
         aa=phi_in(i-1)
         A=30.d0-10.d0*(phi_s(i-1)+(1.d0+beta)*gamma(i-1))+6.d0*phi_s(i
     &        -1)*gamma(i-1)
         do j=0,i-2
            dij=dble(i-j)
            aa=aa+dsqrt(dij-1.d0)*(2.d0*(dij-1.d0)*phi_in(j)-(2.d0*dij+1
     &           .d0)*phi_in(j+1))+dsqrt(dij)*(2.d0*dij*phi_in(j+1)-(2
     &           .d0*dij-3.d0)*phi_in(j))
            A=A+dsqrt(dij-1.d0)*(-30.d0-20.d0*(dij-1.d0)*(phi_s(j)+(1.d0
     &           +beta)*gamma(j))+10.d0*(2.d0*dij+1.d0)*(phi_s(j+1)+(1
     &           .d0+beta)*gamma(j+1))-16.d0*(dij-1.d0)**2*phi_s(j)
     &           *gamma(j)-(16.d0*dij**2+8.d0*dij+6.d0)*phi_s(j+1)
     &           *gamma(j+1)+4.d0*(dij-1.d0)*(4.d0*dij+1.d0)*(phi_s(j)
     &           *gamma(j+1)+phi_s(j+1)*gamma(j)))
            A=A+dsqrt(dij)*(30.d0+10.d0*(2.d0*dij-3.d0)*(phi_s(j)+(1.d0
     &           +beta)*gamma(j))-20.d0*dij*(phi_s(j+1)+(1.d0+beta)
     &           *gamma(j+1))+(16.d0*dij**2-40.d0*dij+30.d0)*phi_s(j)
     &           *gamma(j)+16.d0*dij**2*phi_s(j+1)*gamma(j+1)-4.d0*dij
     &           *(4.d0*dij-5.d0)*(phi_s(j)*gamma(j+1)+phi_s(j+1)
     &           *gamma(j)))
         end do
         aa=aa*2.d0*dsqrt(delt/pi)/3.d0
         A=A*T*dsqrt(delt/pi)/15.d0
```

```
c
c solve nonlinear simultaneous equations
c
c initial guess = solution at previous time step
         x(1)=gamma(i-1)
         x(2)=phi_s(i-1)
         x(3)=phi_in(i-1)
c start loop
         loop=.true.
 10      continue
c evaluate current function values
         f(1)=-(aa+bb*x(3)-x(1))
         f(2)=-(A+B*x(2)+C*x(1)+D*x(2)*x(1)-x(3))
         f(3)=-(sw*x(1)*dsqrt(1.d0-x(2))-dsqrt(2.d0)*(x(2)-x(3)))
c evaluate current Jacobian matrix
         fp(1,1)=-1.d0
         fp(1,2)=0.d0
         fp(1,3)=bb
         fp(2,1)=C+D*x(2)
         fp(2,2)=B+D*x(1)
         fp(2,3)=-1.d0
         fp(3,1)=sw*dsqrt(1.d0-x(2))
         fp(3,2)=-dsqrt(2.d0)-0.5d0*sw*x(1)/dsqrt(1.d0-x(2))
         fp(3,3)=dsqrt(2.d0)
c solve linear equation fp * s = f for s
         ifail=0
         call F04ARF(fp,ia,f,ia,s,works,ifail)
c check size of error
c         print*, s(1),s(2),s(3)
         if (dabs(s(1)) .le. tol .and. dabs(s(2)) .le. tol .and.
     &        dabs(s(3)) .le. tol) loop=.false.
c update solution
         do j=1,3
            x(j)=x(j)+s(j)
         end do
         if (loop) go to 10
```

```
c
c end of nonlinear solve
         gamma(i)=x(1)
         phi_s(i)=x(2)
         phi_in(i)=x(3)
      end do
c
      open(14,file='abel.dat',status='unknown')
      write(14,50)(tt(i),1.d0-phi_in(i),1.d0-phi_s(i),gamma(i),i=0,n)
 50   format(4(f18.9))
c
      end
```

Appendix D

Numerical scheme for the non-static, steady-state nonionic problem

```
function [u,v,W] = convdiff(m, n, cs_0, beta)
dy = 6/m;
dx = 1/n;
m1 = m+1;
m2 = 2*m+2;
m3 = 3*m+3;
nu = dy/(2*dx);
mu = 1/dy;
fprimed_zero = 2*(((beta+cs_0)*(1-cs_0)/cs_0)^2)/pi;
function dw=wprime1(y,w)
dw=[w(2)^2-w(1)*w(3);w(1);w(2)];
yspan = [0:1:100];
wzero = [-0.146; fprimed_zero; 0];
[y,w] = ode45('wprime1', yspan, wzero);
plot(y,w(:,1),'r')
hold on
plot(y,w(:,2),'g')
hold on
plot(y,w(:,3),'b')
c Implicit scheme so stability condition is dx/(dy)^2 <= 1/2
c Initialization
```

```
A = zeros(m3,m3);
B = zeros(m3,m3);
D = zeros(m3,1);
for i = 1:m2/2,
        r(2*i) = 0.01*w(i,2);
        r(2*i-1) = -w(i,3);
end
for i = m2+1:m3,
        r(i) = 1+(cs_0 - 1)*erfc((i-m2-1)*dy*sqrt(fprimed_zero/2));
end
W = r';
v = 0;
c_s(1) = cs_0;
u_s(1) =0;

for t = 2:80,
        A(1,1) = 1;
        for i = 2:m+1,
                A(i,2*i-1) = 1;
                A(i,2*i) = nu;
                A(i,2*i-2) = nu;
                A(i,2*i-3) = -1;
        end
        A(m+2,1) =  2*(dy^2)*(W(m2+1)-v)/(beta+v);
        A(m+2,4) = -4*dx;
        A(m+2,2) = 4*dx+2*(dy^2)*W(2);
        A(m+2,m2+1) = 4*dy/(beta+W(m2+1));
        for i = m+3:m2-1,
                A(i,2*(i-m)-4) = -mu;
                A(i,2*(i-m)-3) = (W(2*(i-m)) - W(2*(i-m)-4))/2;
                A(i,2*(i-m)-2) = 2*(mu + nu*W(2*(i-m)-2));
                A(i,2*(i-m)) = -mu;
        end
        A(m2,m2) = 1;
        A(m2+1,2) = -4*dy*W(m2+1)/(beta+W(m2+1));
        A(m2+1,m2+1) = -(4*dx+2*(dy^2)*W(2))-(4*dy*W(2)/(beta+W(m2+1)))
```

```
                    +4*dy*(W(2)*W(m2+1)/((beta+W(m2+1))^2));
        A(m2+1,m2+2) = 4*dx;
        for i = m2+2:m3-1,
                A(i,2) = (i-m2-1)*(dy^2)*(W(i+1)-W(i-1));
                A(i,i-1) = 2*dx;
                A(i,i) = -(4*dx+2*(dy^2)*W(2));
                A(i,i+1) = 2*dx;
        end
        A(m3,m3) = 1;

        for i = 2:m+1,
                B(i,2*i-2) = nu;
                B(i,2*i) = nu;
        end
        B(m+2,2) = 2*(dy^2)*W(2);
        B(m+2,m2+1) = 4*dy/(beta+W(m2+1));
        for i = m+3:m2-1,
                B(i,2*(i-m)-2) = 2*nu*W(2*(i-m)-2);
        end
        B(m2+1,2) = (-2*(dy^2)-(8*dy/(beta+W(m2+1)))
                    +(4*dy*W(m2+1)/((beta+W(m2+1))^2)))*W(m2+1);
        for i = m2+2:m3-1,
                B(i,i-1) = -(i-m2-1)*(dy^2)*W(2);
                B(i,i) = -2*(dy^2)*W(2);
                B(i,i+1) = (i-m2-1)*(dy^2)*W(2);
        end

        D(m3,1) = 1;

c Au = BW +D

        C = A \ B;
        E = A \ D;
        u = C*W + E;
        v = W(m2+1);
        W = u;
```

```
        c_s(t) = W(m2+1);
        u_s(t) = W(2);
end

for i = 1:m1,
        c(i) = u(m2+i);
end
for i = 1:m2/2
          u_vel(i) = u(2*i);
end
j = linspace(0, 6, m2/2);
figure(1)
plot(j, u_vel);
hold on
figure(2)
plot(j, c);
hold on
x = (0:79)*dx;
figure(3)
plot(x, c_s)
hold on
figure(4)
plot(x, u_s)
hold on
```

Bibliography

[1] D.J. Acheson. *Elementary fluid dynamics*. Oxford, 1990.

[2] Z. Adamczyk, G. Para, and P. Warszyński. Influence of ionic strength on surface tension of cetyltrimethylammonium bromide. *Langmuir*, 15:8383–8387, 1999.

[3] A.W. Adamson. *Physical chemistry of surfaces*. New York: Wiley, 4th edition, 1982.

[4] P.W. Atkins. *The Elements of Physical Chemistry*. Oxford, 1992.

[5] C.D. Bain, S. Manning-Benson, and R.C. Darton. Rates of mass transfer and adsorption of hexadecyltrimethylammonium bromide at an expanding air-water interface. *Journal of Colloid and Interface Science*, 229:247–286, 2000.

[6] B.I. Bleaney and B. Bleaney. *Electricity and magnetism*. Oxford, 1994.

[7] C.J.W. Breward, R.C. Darton, P.D. Howell, and J.R. Ockendon. The effect of surfactants on expanding free surfaces. *Chem. Eng. Sci.*, 56:2867–2878, 2001.

[8] C. Chang and E.I. Franses. Adsorption dynamics of surfactants at the air/water interface: a critical review of mathematical models, data, and mechanisms. *Colloids and Surfaces*, 100:1–45, 1995.

[9] S.S. Datwani and K.L. Stebe. The dynamic adsorption of charged amphiphiles: the evolution of surface concentration, surface potential, and surface tension. *Journal of Colloid and Interfacial Science*, 219:282–297, 1999.

[10] V. Dudnik and K. Lunkenheimer. Dynamic surface potential and adsorption kinetics of nonionic surfactants at the air-water interface. *Langmuir*, 16:2802–2807, 2000.

[11] G. Geeraerts, P. Joos, and F. Villé. Dynamic surface tension and dynamic surface potentials of aqueous solutions of a cationic surface active electrolyte. *Colloids andf Surfaces*, 95:281–291, 1995.

[12] P.D. Howell and C.J.W. Breward. Mathematical modelling of the overflowing cylinder experiment. *J. Fluid Mech.*, 2001.

[13] S. Manning-Benson, C.D. Bain, and R.C. Darton. Measurement of dynamic interfacial properties in an overflowing cylinder by ellipsometry. *Journal of Colloid and Interfacial Science*, 189:109–116, 1997.

[14] S. Manning-Benson, C.D. Bain, R.C. Darton, D. Sharpe, J. Eastoe, and P. Reynolds. Invasive and non-invasive measurements of dynamic surface tensions. *Langmuir*, 13:5808–5810, 1998.

[15] S. Manning-Benson, S.W.R. Parker, C.D. Bain, and J. Penfold. Measurements of the dynamic surface excess in an overflowing cylinder by neutron reflection. *Langmuir*, 14:990–996, 1998.

[16] M. Mulqueen and D. Blankschtein. Prediction of equilibrium surface tension and surface adsorption of aqueous surfactant mixtures containing zwitterionic surfactants. *Langmuir*, 16:7640–7654, 2000.

[17] H. Ockendon and J.R. Ockendon. *Viscous Flow*. Cambridge: Cambridge University Press, 1995.

[18] J. Ockendon, S. Howison, A. Lacey, and A. Movchan. *Applied partial differential equations*. Oxford, 1999.

[19] H.A. Priestley. *Introduction to complex analysis*. Oxford, 1995.

[20] D.F. Schriver, P.W. Atkins, and C.H. Langford. *Inorganic chemistry*. Oxford, 1994.

[21] I.U. Vakarelski and C.D. Dushkin. Effect of the counterions on the surface properties of surfactant solutions: kinetics of the surface tension and surface potential. *Colloids and Surfaces*, 163:177–190, 2000.

[22] P.M. Vlahovska, D.D. Krassimir, A. Mehreteab, and G. Broze. Adsorption kinetics of ionic surfactants with detailed account for the electrostatic interactions. *Journal of Colloid and Interfacial Science*, 192:194–206, 1997.